PROCESS DEVELOPMENT FOR HIGH SPEED TRANSISTOR LASER OPERATION

BY

ADAM L. JAMES

DISSERTATION

Submitted in partial fulfillment of the requirements
for the degree of Doctor of Philosophy in Electrical and Computer Engineering
in the Graduate College of the
University of Illinois at Urbana-Champaign, 2010

Urbana, Illinois

Doctoral Committee:

Professor Milton Feng, Chair
Professor Nick Holonyak Jr.
Professor Jianming Jin
Professor José Schutt-Ainé

ABSTRACT

The transistor laser (TL) offers advantages over conventional diode laser structure. The TL uses high base doping and minority carrier collection to reduce the recombination lifetime in the active region of the device to <30 ps. A fast recombination lifetime <30 ps reduces the photon-carrier resonance when modulating the device at RF frequencies. However, the transistor laser with high intrinsic optical speed is limited by more than just internal recombination lifetime; it is also limited by parasitic resistances and capacitances. Small signal bandwidth of 20 GHz and digital modulation of 20 Gbit/s was obtained by reducing or eliminating extrinsic parasitics which limit device performance through the optimization of device geometry and process conditions.

To my family

ACKNOWLEDGMENTS

I would like to thank my adviser, Professor Milton Feng, for the opportunity to become a member of his research group and for his continuous support and guidance throughout my graduate school career. Not only has his support been crucial to this work, but also I am grateful that Professor Feng always provides extra motivation to get things done. I would like to thank Professor Nick Holonyak Jr. for giving me the direction on each and every development stage of the transistor laser. I greatly benefited from his philosophy and method of performing the pioneering research work. In addition, I would also like to thank Professors Keh-Yung Cheng and Kuang-Chien Hsieh for guiding me and for productive discussions. I would like to thank Professors Jianming Jin and José Schutt-Ainé for serving on my doctoral committee. I benefited from a research environment that allowed me to broaden my horizons, and the opportunity to work in the High Speed Integrated Circuits (HSIC) Group has been a great privilege. This work would not have been possible without the mentoring of Dr. Gabriel Walter, Dr. Richard Chan, Dr. Benjamin Chukung, and Dr. Walid Hafez. Their expertise in laser and transistor fabrication processes and high-frequency optoelectronic measurements made the completion of the work possible.

I want to thank to our transistor processing team members Dr. Forest Dixon, Kurt Cimino, Dr. William Snodgrass, Donald Cheng, Wayne Wu and Dr. Han-Wui Then for their assistance in the fabrication process and device characterization. Thanks also to all

of the present and past group members: Mark Stuenkel, Fei Tan, Mong-Kai Wu, and Rohan Bambery. Their mentoring, hard work, and friendship have made the HSIC group a pleasant place for academic research. I would like to thank R. A. Athale (DARPA/MTO) for the support of DARPA Contract No. HR0011-04-1-0034 (Hyper-Uniform Nanophotonics Technologies, HUNT Center). I would like to thank Dr. William Grande for my first introduction to what a semiconductor can do and his excellent non-conventional treatment of the subject; it was integral in my choice to pursue research in III-V semiconductors. I would also like to thank Dr. Athimoottil Mathew of Rochester Institute of Technology for his advice, guidance and rigorous standards during my undergraduate career, showing me that achieving anything is possible with hard work and dedication. Above all, I would like to thank my family and relatives for their endless support. I cannot express enough gratitude to my family, and I dedicate this dissertation to them.

TABLE OF CONTENTS

CHAPTER 1

INTRODUCTION

A problem facing the microelectronics industry is the speed at which signals can be transmitted from device to device (either on chip or off chip). Conventional data transmission is dominated by metal interconnects which are limited by parasitic loss and RLC (resistance, inductance, and capacitance) time constants. It has been widely proposed that optical interconnects are an advantageous replacement for metal transmission lines. However, one main problem with optical interconnects is not the bandwidth provided by optical transmission or even waveguide loss, but the available sources which can be integrated and have a bandwidth greater than that of metal interconnects. If a high speed source can be realized, optical interconnect systems hold the promise to decouple system performance from transmission line resistances and capacitances, effectively eliminating the propagation RC time constant.

If quantum well (QW) lasers diodes (LDs) are used for high-speed direct modulation of optical signals, there is no clear advantage over traditional metal interconnects, since laser diode bandwidth is limited to several gigahertz with the additional complication of a carrier-photon resonance; this limitation in current diode lasers is caused by the dynamics of recombination and device design. The diode accumulates a large amount of charge in the active region (maintaining population inversion) and is unable to unload the charge quickly, limiting the modulation speed. Carriers are contained by heterojunction barriers while they

wait to recombine (lifetime $\sim$ 1 ns). To increase the modulation speed, a larger population (more charge) is required to enhance the recombination lifetime through stimulated emission. If a diode is driven far above threshold, a certain amount of charge is stored; therefore, when the laser is turned off the only process to reduce the population is recombination, leading to a slow turn-off.

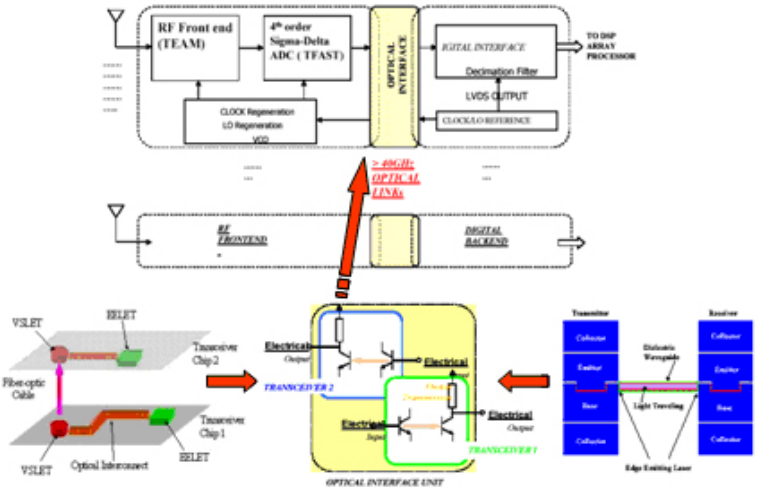

Figure 1.1: Proposed network topology for optical interconnects [1].

A possible solution to the high speed interconnect problem is the use of an electro-absorption modulator (EA). The EA solution requires large voltages in excess of 7 V for operation. External modulators have low power efficiency, a DC laser must be powered (same as diode laser), and also the modulator must be powered. The diode and modulator combination is also a large structure due to the length of absorption material needed to quench the optical signal. Integration on a chip requires each element to be small and not use an inordinate amount of power (reduce localized heating). The proposed solution (Figure 1.1) is the use of a light emitting transistor which does not store charge in the active region but sweeps out carriers through the collector. A transistor is based on a short based topology; if a carrier is not recombined it is swept from the recombination region (base). The transistor laser topology holds promise to solve the above problems. Transistors are not limited to 30 GHz as are laser diodes, but can be operated in excess of 100 GHz.

A transistor can also be used at lower rail voltages. In order to develop an ultrafast light source (transistor laser, TL) and resulting system (Figure 1.1), the following abilities must be developed: transistor fabrication art to eliminate parasitic capacitances and resistances (to avoid the problem which is limiting electrical interconnects), high speed electrical layout, device modeling through the use of electrical scattering parameters, and an understanding of transistor operation.

CHAPTER 2

TRANSISTOR OPERATION

2.1 Historical Development

Prior to the invention of the transistor in 1947 (Bardeen and Brattain [2]) semiconductor rectification was known and utilized (metal-semiconductor junction)[3]; however, the importance of the hole as a conducting element was not appreciated. An understanding of the interaction between electrons and holes in a semiconductor is necessary to recognize how the transistor is able to perform the remarkable feat of low impedance signal injection and high impedance extraction. The conductivity of a semiconductor is proportional to the amount of free carriers in the material.

> "In a semiconductor containing substantially only one type of current carrier, it is impossible to increase the total concentration by injecting carriers of the same type; however, such increases can be produced by injecting the opposite type since the space charge of the latter can be neutralized by an increased concentration of the type normally present"(W. Shockley)[4].

In order to modulate material conductivity, electrons and holes are required, as well as a sink for their currents provided by electron/hole recombination (a transistor also using a current collector). Recombination allows for the continuous injection of current from the

emitter to the base and photon emission from direct band-gap materials. Light emission from recombination can be contained in a resonating volume causing stimulated emission (coherent optical field), an operation historically performed by a laser diode [5]. A transistor, however, uses the recombination/base current to cause carrier injection into the base, and then "tricks" the injected carriers by removing them from the recombination (base) region before they are able to recombine (in contrast to the laser diode, where ideally all carriers recombine). Figure 2.1 shows a schematic image of a transistor laser with carrier flow indicated. Carriers injected into the base that do not recombine are collected, typically by a reverse biased pn junction. Transistors normally sacrifice a small amount ($\sim$1%) of emitter current to achieve base-to-collector current gain. Transistor operation involves recombination; therefore, a transistor fabricated from direct-gap materials can emit photons.

2.2 Quantum Well Light Emitting Transistor

An InGaP/GaAs heterojunction bipolar transistor (HBT) was observed to emit photons [6]; the device is then reengineered with a quantum well in the base [7] to enhance the optical gain. The quantum well (QW) in the base provides a recombination center, restricts the output optical spectrum, and regulates the amount of recombination in the base. When recombination is increased the quantity of injected carriers reaching the collector is reduced, lowering the common emitter gain. Once a transistor is altered enough to have optical gain, it is possible to confine the optical output in a resonant cavity to produce stimulated emission, thus realizing a transistor laser (TL) (Figure 2.1).

Just as understanding a transistor required the concept of the hole, the transistor laser cannot be understood without the photon. The transistor laser ties the electron, hole, and photon (previously not generated in a transistor) together in a three-terminal device allowing an additional dimension of output characterization compared to a laser diode (V_{CE}, electrical) and conventional transistor (photon readout). The transistor laser is also being

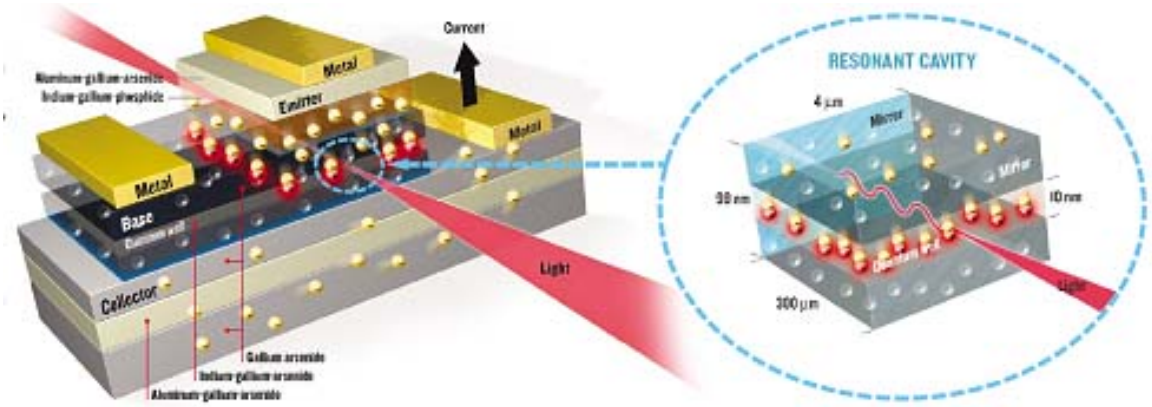

Figure 2.1: Schematic image of transistor laser and current flow through the device [8].

developed on a platform (GaAs) where transistor modulation speeds have reached over 100 GHz, while laser diodes achieve 10 GHz. The TL promises to deliver modulation speeds in between, which would be an improvement over existing directly modulated optical sources, allowing for their incorporation into the telecommunications infrastructure and on-chip optical interconnects to replace parasitically limited RLC transmission lines. The presented work is to characterize the electron, hole, and photon interactions in the transistor laser, and to improve the device characteristics with an emphasis on increasing modulation speed.

CHAPTER 3

FIRST GENERATION FABRICATION

In order to develop a process to fabricate a semiconductor device, the material structure must be known, as well as the physical chemistry to etch the crystal. Figure 3.1 is a layer structure representative of a transistor laser, around which the following process is developed. The fabrication process must be developed in conjunction with physical layout to ensure that the process will succeed, the device will operate as desired, and the electrical performance will improve.

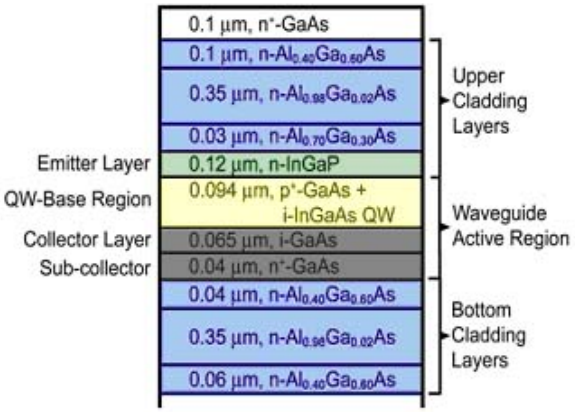

Figure 3.1: Crystal structure representative of a transistor laser [9].

The first generation devices built to test the feasibility of a transistor laser are not optimized for high speed operation. The original process for the fabrication of a transistor laser is shown in Figure 3.2. The process (after etching the emitter) advantageously oxidizes an AlxGa(1-x)As layer to separate the semiconductor from the signal metallization. The layout, however, is problematic from an RF standpoint. The oxide forms a large capacitance between electrodes. At high frequencies the impedance of the capacitor drops; the signal is no longer transmitted into the device but rather around the device (parallel path). Another RF difficulty arising from crystal growth is a 0.5-μm-thick conductive buffer layer underneath the bottom cladding layers. The conductive layer is a lossy material and contributes heavily to signal attenuation. The removal of the alumina layer, underlying base, collector, cladding, and buffer layers presents a large technical difficulty to the fabrication of the structure. The material removal results in a 2-μm-deep topography, which emitter, base, and collector metal must traverse. The additional constraint that metallization must not extend around the edges of the device is also imposed (metallization must not interfere with facet cleave). At this juncture there are two possible ways to traverse the gap: either run the metal along the bottom of the trench or fill the trench and deposit the metal above the fill.

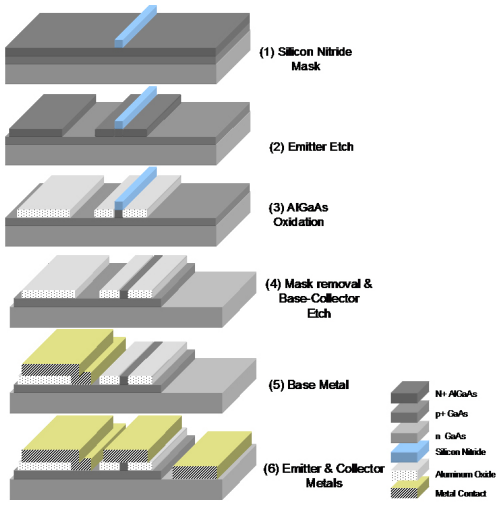

Figure 3.2: Edge emitting HBLET fabrication process flow using stripe laser geometry [1].

The design considerations are the compatibility of the process to future crystals, the

feasibility of implementation, and the flexibility of the design. In order to fabricate the device with the metal along the bottom of the trench, much care must be taken not to short the base to the collector as the base metal extends across the collector. Base metal traversing the collector is unavoidable due to the location of the base. The decision was made to fill the gap and run the metal over the filled region. The first generation devices used a layer of polyimide to separate the emitter metal and base metals. The fact that polyimide forms a conformal coating presents a grave topological problem. When spun on, the trench will fill 2 μm, but also increase the height of the emitter by 2 μm. A low permittivity planarizing dielectric, BCB (benzocyclobutene), is chosen instead. During test experiments the polymer reduces the topography from 2 μm to 100 nm, an acceptable distance for contact lithography. However, the BCB spins on 4-μm-thick, overfilling the trench; 2 μm must be etched away to expose the emitter for metallization. The complete proposed transistor laser fabrication process is shown in Figure 3.3.

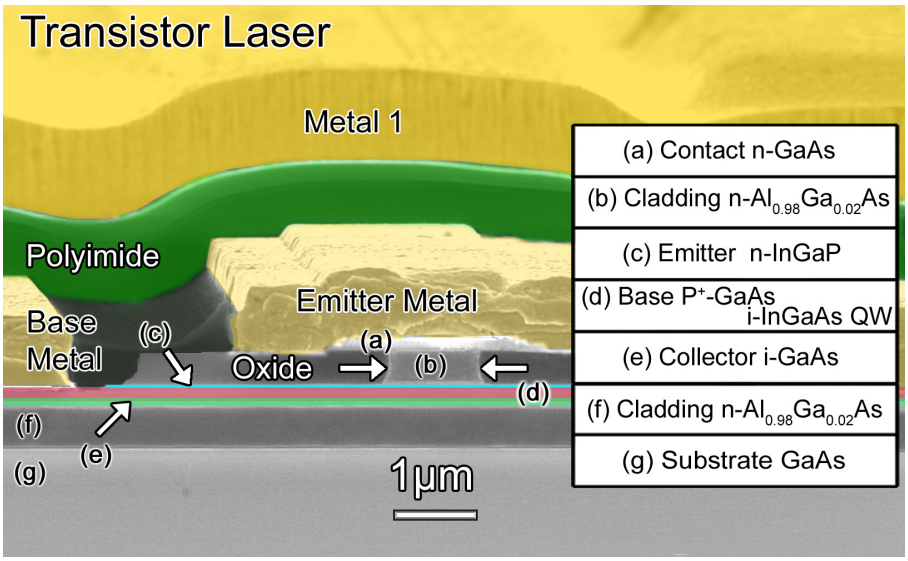

Figure 3.3: False-color SEM micrograph of transistor laser facet with emitter, base, and collector regions identified.

The process uses 12 mask levels and yields a final device height of 4.25 μm. The process begins with photolithography, defining the emitter of the TL (Figure 3.3 step 1). A two-step

etch is used: the first step to remove GaAs and low Al content layers (citric acid: H_2O), the second ($H_2SO_4 : H_2O_2 : H_2O$) (Figure 3.3 step 2) to clear the aluminum bearing layers stopping selectively on the InGaP emitter. The emitter contact metal (AuGe/Ni/Au also used for collector contacts) is then deposited through a bilayer masking resist and lifted off (all metals are deposited similarly). The emitter is then etched using HCl allowing contact metallization of Ti/Pt/Au to bare material. The GaAs base is etched using the same citric acid as above, exposing the collector material. Collector ohmic metal is deposited along with a Ti/Au layer which extends from the collector to the level of the emitter. This step is performed at this stage of the process to avoid lithography problems (large step height) after the collector, cladding, and buffer layer are removed (Figure 3.3 step 3). The collector and buffer layers are removed by a sulfuric:peroxide etch. Electrical verification is performed to ensure that the etch has indeed reached the semi-insulating substrate. If the semi-insulating substrate is not reached, all pads will be shorted by the remaining unetched material. The decision to anchor the pads to semi-insulating substrate is made to allow for the possibility of wire bonding. If the pad is anchored on an insulator instead of being alloyed to the semiconductor, the bond pads will be ripped from the surface during bonding. Next the BCB is spun on, filling the void caused by the isolation etch, planarizing the surface. The BCB layer is then etched in a reactive ion etcher by CF4 to the emitter level. Metal 1 and Post 1 are deposited; the BCB process is repeated, allowing for the final deposition of metal, Metal 2.

CHAPTER 4

DEVICE CHARACTERIZATION

4.1 Transistor Laser DC Operation

The most notable difference between a conventional transistor structure (HBT) and TL is the insertion of a quantum well into the base region, and the thick emitter/collector cladding layers. By adding a QW, less emitter current is transported to the collector because of enhanced recombination. If I_E is held constant given $I_C = \beta \times I_B$ (current gain) and $I_E + I_C + I_B = 0$ (continuity of current), while I_B is increased, then I_C decreases, reducing the common emitter gain $\beta \equiv \Delta I_C / \Delta I_B$ and related $\alpha \equiv \Delta I_C / \Delta I_E$. A conventional HBT has a β value that is close to 100. After a quantum well is inserted, the gain drops dramatically to the range of 1 to 10. If the optical feedback is sufficient, the device shifts recombination processes from spontaneous operation to stimulated emission, and the gain compresses, reducing β (Figure 4.1(a) region 2) further than just QW insertion. As I_B is increased in region 1 of Figure 4.1(a), the collector current begins to compress (region 2), showing the onset of stimulated emission. The interface between regions 1 and 2 in Figure 4.1(a) is the threshold base current, I_{TH}.

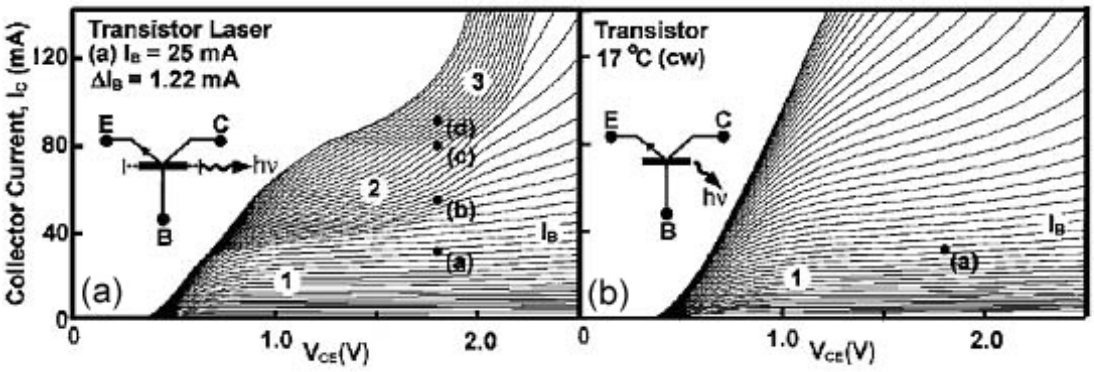

Figure 4.1: Collector I-V characteristics (a) of an n-p-n InGaP/GaAs/InGaAs(QW)/GaAs heterojunction bipolar transistor (HBT) laser with decreased gain ($\beta \equiv \Delta I_C/\Delta I_B$) in the stimulated emission regions (2) and (3) compared to (b) ordinary transistor operation with cavity Q spoiled (region (1), spontaneous recombination, $\beta_{ST} < \beta_{SP}$)[10].

4.2 Transistor Laser with Reduced Cavity Q

To confirm that stimulated emission changes the structure of the electrical output, a condition for stimulated emission can be changed and differences in the collector output observed. Laser threshold (general) is determined by the optical gain, the length of the gain path, and mirror reflection (cavity Q). In one experiment the cavity Q is reduced by coating a facet of a TL with an alumina paste; the small size and randomness of the particles (~ 0.05 μm) scatter the optical field, precluding the possibility of optical feedback. The device immediately shifts from stimulated to spontaneous emission, and uncompressed HBT characteristics (Figure 4.1(b)). A second region of operation (Figure 4.1(a) region 3) with different gain compression exists at higher base currents. As the base current is increased (from Figure 4.1(a) region 2 to region 3) the device shifts optical wavelength from ~ 1 μm to ~ 970 nm. The wavelength and corresponding λ shift are due to the quantization effect of the QW on the available density of states. For a simplified argument: the number of carriers is equal to the integral of density of states (DOS) as a function of energy, D(E), and the Fermi function, $f(E)$ (probability of finding a carrier at an energy), $n = \int D(E)f(E)dE$. In order for the carrier level to increase, energy must also increase. The QW density of states is step-like

(bounded by the bulk DOS) and pins the optical transition at geometrically controlled energy levels; the lowest bound state of this well has $\lambda = 1$ μm (Figure 4.2 (b)). As the number of carriers is increased, the probability of finding a carrier in the second bound state increases. When the competition from the second state transition is no longer negligible, multimode operation ($\lambda = \sim 980$ nm and 1 μm) occurs (Figure 4.2 (c)). Further increase in carrier density results in second state domination, and reduction of the 1-μm lasing mode (Figure 4.2 (d)).

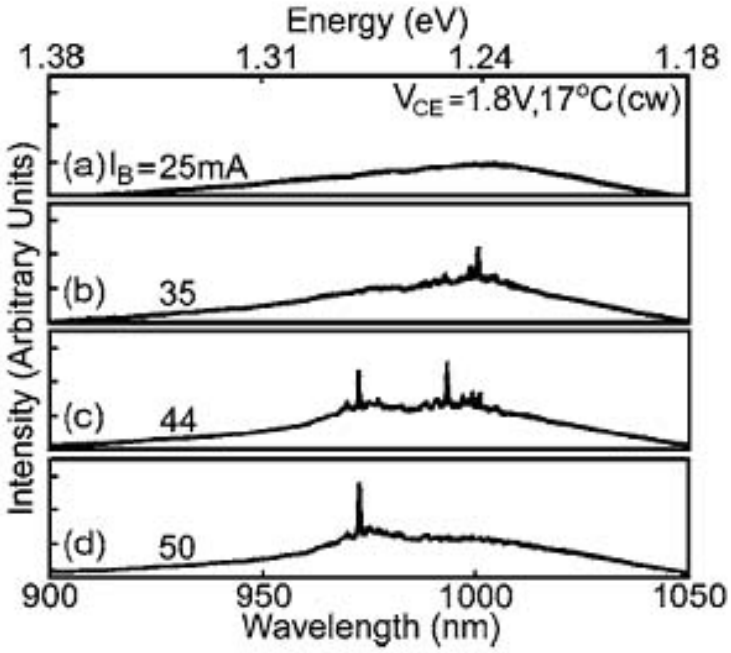

Figure 4.2: Recombination radiation spectra (spontaneous and stimulated) of the transistor laser A of Figure 4.1 ($V_{CE} = 1.8$ V) at the base current bias points (a) $I_B = 25$, (b) 35 , (c) 44, and (d) 50 mA [10].

4.3 First-Order Charge Control Analysis

Even though the device is using stimulated base recombination, transistor analysis techniques apply [10], including charge control analysis [11]. If the introductory arguments about transistor operation are continued, then when a hole is injected into the base from the base

contact, an electron must also be injected into the base from the emitter to maintain spaced charge neutrality. The electron diffuses across the base to the collector in time, τ_t (transit time); then the emitter must continue injecting carriers to compensate for the injected hole until the hole has been recombined, τ_b (recombination lifetime). We take the ratio τ_b/τ_t as the average number of electrons transferred to compensate the charge of the hole until a recombination event, giving $I_C = I_B\tau_B/\tau_t$ and $\beta = \tau_B\tau_t$. From the above lifetimes the port currents can be written

$$I_E = I_B + I_C = \frac{Q_B}{\tau_B} + \frac{Q_B}{\tau_t}, \tag{4.1}$$

where Q_B is the charge stored in the base. For an ordinary InGaP/GaAs HBT with a base thickness of 100 nm, a doping concentration of 10×10^{17} cm^{-3}, and typical current gain $\beta = 100$, we estimate $\tau_t = W_B^2/2D = 1.93$ ps and $\tau_b = \beta \times \tau_t = 193$ ps. For the same HBT with a quantum well inserted in the base, a QWHBT, the base current and β gain can be modified and expressed as

$$I_B = \frac{Q_B}{\tau_B} + \frac{Q_b}{\tau_{QW}} = \frac{Q_B}{\tau_t}, \beta = \frac{\tau_{BQW}}{\tau_t}, \tag{4.2}$$

where τ_{QW} is the recombination lifetime of the quantum well and τ_{BQW} is the combined recombination lifetime. Figure 4.3 (curve B) shows the differential gain at $V_{CE} = 1.8$ V (spontaneous recombination for the Q spoiled TL); the current gain β_{QW} is measured to be 4.2, 8.5, and 14 for base current values I_{BQW} of 35, 44, and 50 mA, respectively, yielding an estimate for $\tau_{QW} = \beta_{QW}\tau_t = 8.1$, 16.4, and 27 ps.

For a transistor laser (TL) with stimulated base recombination, the base current and current gain can be further modified and expressed as

$$I_B = \frac{Q_b}{\tau_B} + \frac{Q_B}{\tau_{QW}} + \frac{Q_B}{\tau_{ST}} = \frac{Q_B}{\tau_{TL}}, \beta = \frac{\tau_{TL}}{\tau_t}, \tag{4.3}$$

where τ_{TL} is the effective base recombination lifetime of the transistor laser including τ_{ST},

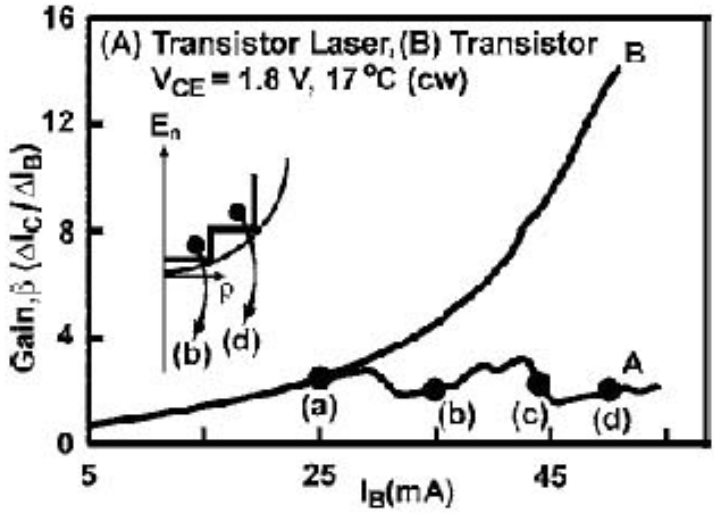

Figure 4.3: Gain values β of the transistor laser A of Figure 4.1 ($V_{CE} = 1.8$V) shown in comparison to B ordinary transistor operation at the same I_B bias values (a), (b), (c), and (d) shown [10].

the stimulated recombination lifetime. In Figure 4.3 the TL gain values are (b) $\beta_{TL} = 2$, (c) 2.2, and (d) 2 for $I_B = 35$, 44, and 50 mA, respectively. Hence, the corresponding τ_{TL} values are calculated as 3.9, 4.3, and 3.9 ps. From these τ_{TL} the following values for the stimulated recombination lifetimes are obtained: (b) $\tau_{ST} = 7.4$ ps ($I_B = 35$ mA, first bound state), (c) 5.8 ps ($I_B = 44$ mA, first and second bound state transition), and (d) 4.5 ps ($I_B = 50$ mA, second bound state). At higher base current and more band filling, laser operation at shorter wavelength (higher energy) occurs at higher speed (to be confirmed with small signal modulation data), agreeing with the higher density of QW states at higher energy.

4.4 Transistor Laser with Enhanced Cavity Q

Since the collector IV characteristics of the transistor laser are affected by reducing the cavity Q preventing stimulated emission, enhancing the cavity Q should enhance the stimulated emission process. A $Ga_{16.5}In_{83.4}$ eutectic (liquid at room temperature) is coated onto one facet. Optical spectra and IV characteristics are taken before (Figure 4.4, curve 1) and after

the facet was coated (Figure 4.4, curve 2).

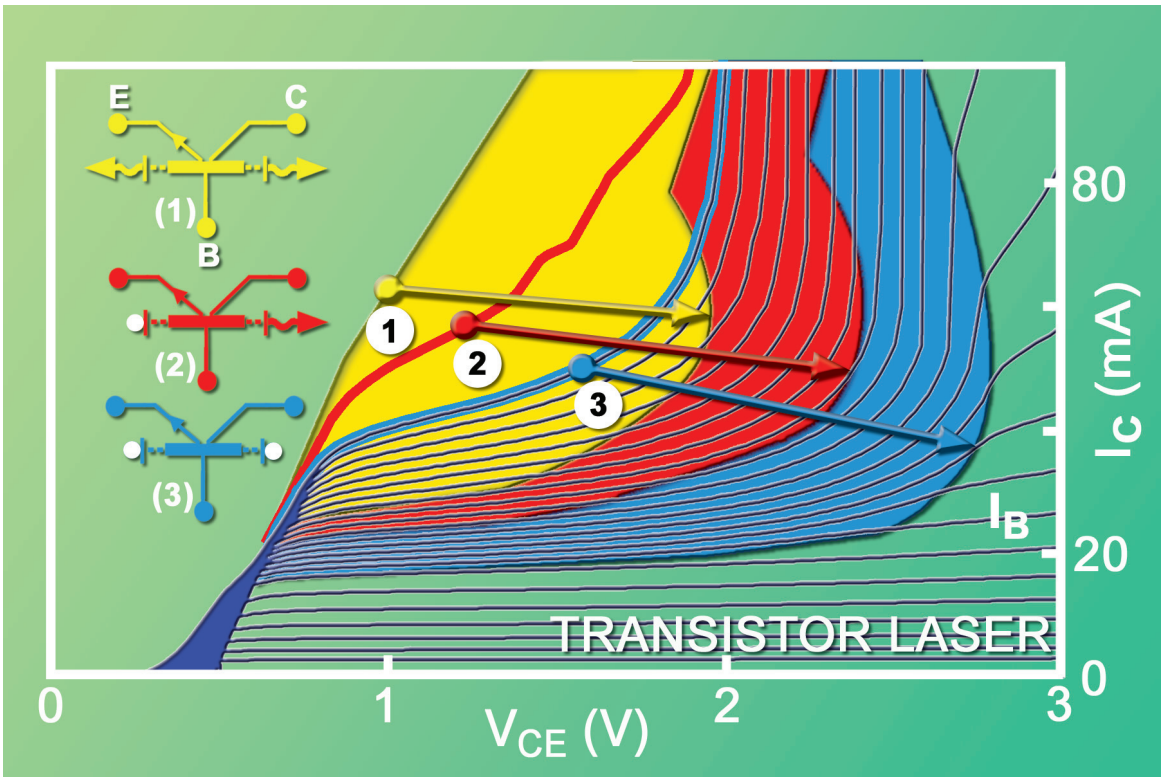

Figure 4.4: Collector I-V characteristics of a transistor laser: (1, light gray) as cleaved, (2, darkest gray) single mirror enhanced, and (3, gray) two-mirrors enhanced [12].

No substantial optical power is detected after the facet is coated, but optical data is still able to be taken from the uncoated facet. With the first facet coated, the threshold current reduces and the stimulated operational voltage range extends compared to uncoated operation. The second facet is then coated, removing completely the ability to take spectral data; however, from the collector I-V characteristics the threshold is seen to reduce, and again, the voltage range extends (Figure 4.4, curve 3). Looking at the breakdown (right side Figure 4.4) region of the I-V family, the gain compression reduces and returns to uncompressed characteristics. The boundary created by an abrupt slope change in I_C demarcates a shift in operation from stimulated to spontaneous emission with increasing V_{CE}. The operational voltage range extends as I_B is raised from I_{TH}. At a certain value the operational range cuts back to lower values of V_{CE} until the stimulated transition switches to the second bound

state. With both mirrors coated, the device runs with a low threshold (low optical strength); increasing I_B produces a higher optical field strength. At high field strength the device shifts from a high coherent optical field to a lower average field (Figure 4.5).

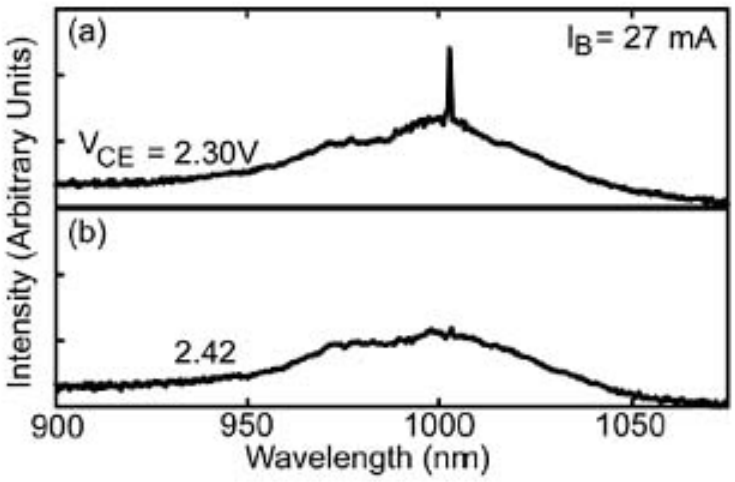

Figure 4.5: Recombination radiation spectra [(a), stimulated and (b), spontaneous] of the transistor laser of Figure 4.4 (I_B = 27 mA) at (a) V_{CE} = 2.30 and at (b) 2.42 V with, for (b), the high-field photon-assisted tunneling reduced or quenched (the sharp mode) by the constraint $I_E + I_B + I_C = 0$ as $\alpha \to 1$ ($\alpha \equiv \Delta I_C/\Delta I_E$) [12].

This behavior is consistent with Franz-Keldysh (FK) (photon-assisted tunneling, Figure 4.6(b), in contrast with tunneling Figure 4.6(a)) absorption (used in electroabsorption modulators), and three-terminal conservation of current. As the magnitude of the electromagnetic field in the device increases, the energy bands bend, thus allowing the wave-functions to penetrate into the energy gap. The breakdown of Zener diodes occurs as the carrier wave function extends into the gap, allowing the carrier to traverse an energy barrier. The Franz-Keldysh effect occurs at field strengths greater than $\sim 10^4$ V/cm, allowing absorption of lower energy photons, below the unbiased band edge. This allows the absorption of higher energy photons (still below the band gap) at lower bias fields than lower energy photons (further below gap energy). At shorter wavelengths the maximum operational voltage range will be lower for the same collector structure (supported by the second bound state transition operational range).

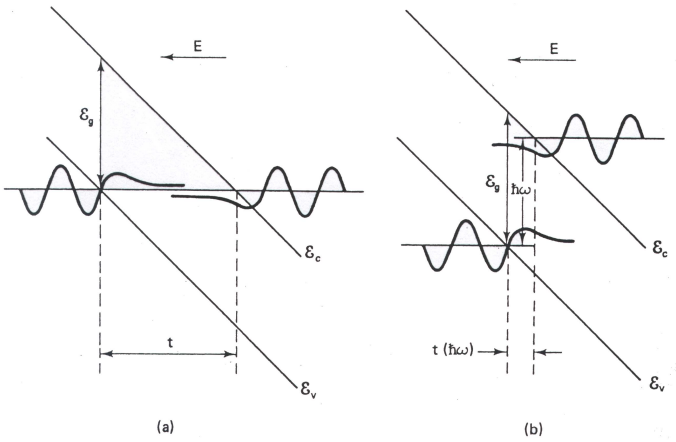

Figure 4.6: Energy band diagram in an electric field showing wavefunction overlap (a) without and (b) with the absorption of a photon of energy [13].

Note that the electromagnetic field specified is the superposition of the DC bias field and the high frequency optical field; thus an increase in photon density is equivalent to an increase in bias field strength, which allows the device to shift from stimulated emission (large coherent field) to spontaneous emission (lower average field) and maintain conservation of current $I_E + I_B + I_C = 0$. We can see in region 3 of Figure 4.4 that the characteristics curve upward toward an infinite slope, $\beta \to \infty$ and $\alpha \to 1$. In a transistor $\alpha = 1$ implies that all emitter current is traversing the base to the collector. In the case where the device is driven in stimulated emission, the hole current and recombination cannot be ignored. The recombination shifts from stimulated (high field) to spontaneous (low average field) to rebalance the currents away from the $\alpha \to 1$ condition. If it is increased further, the bias field will compensate for the optical field lost in switching from stimulated to spontaneous emission, and the device will again approach the $\alpha \to 1$ condition, leading to final breakdown of the device. Breakdown is dependent not only on the electrical bias field but also on the optical field strength, yielding a photon-assisted breakdown mechanism in the TL (and perhaps all direct-gap recombination transistors).

4.5 Transistor Laser Modulation Bandwidth

The performance of an HBT is closely tied to device processing and geometrical layout, which control the elimination of parasitic resistances and capacitances. The first generation transistor lasers exhibit a 3-dB optical bandwidth of 13.5 GHz for a 400-μm gain path. The TL bandwidth varies substantially from conventional laser diode bandwidth; there is no noticeable resonance peak, and bandwidth is dependent on the QW DOS. The optical bandwidth was measured using a New Focus 1414 25 GHz detector, and 20 GHz traveling wave amplifier; a signal at a given frequency is input into the device, and the resultant optical amplitude at frequency is measured, as shown Figure 4.7.

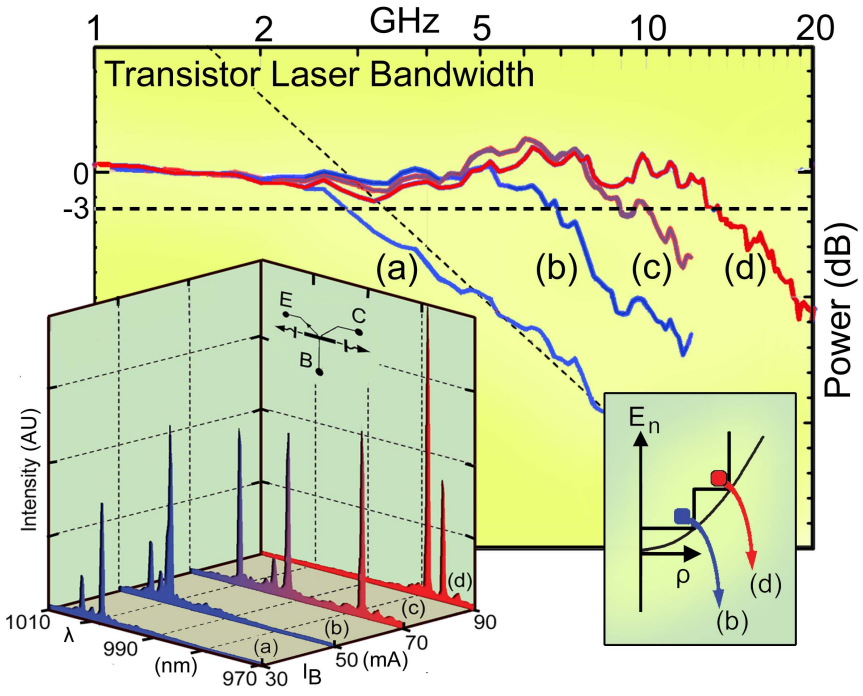

Figure 4.7: Right inset: Recombination radiation spectra of the transistor laser of (V_{CE} = 1.5 V) at the same base current bias points: (a) I_B = 30 ($\lambda = 1\mu$m), (b) 50 , (c) 70 (λ= 1 and 0.98 μm), and (d) 90 mA. Main: Frequency response of the transistor laser (V_{CE} = 1.5 V, I_{TH} = 23 mA) at the base bias currents: (a) I_B/I_{TH} = 1.3, (b) 2.2, (c) 3.0, and (d) 3.9. Note the "flat" response, no carrier-photon resonance peak. Left inset: Quantum well state transitions [14].

4.6 Bandwidth Analysis

An analysis of the modulation frequency response of the transistor laser can be derived from an extension of the coupled rate carrier-photon equations formulated by Statz and deMars (1960)[15]. The modulation frequency response $M(\omega)$ can be expressed as

$$M(\omega) = \frac{\Delta P_m}{\Delta J_B} = \frac{(\tau_p/ew_b)}{[1-(\omega/\omega_n)^2] + j2(\omega/\omega_n)\xi}, \tag{4.4}$$

where ΔP_m is the modulated photon density and ΔJ_B is the modulated base current density. The natural undamped frequency, ω_n, can be estimated from the photon lifetime and recombination lifetime for a given base current to threshold current ratio employing the expression $\omega_n \approx (1/\tau_B\tau_p)[(J_B/J_{TH}) - 1))$. The damping ratio, ξ, can then be calculated from the undamped frequency, the photon lifetime, and the base recombination lifetime via the relationship $\xi = (1/2)((1/\omega_n\tau_B) + (\omega_n\tau_B))$. The photon lifetime can be obtained from the usual expression $1/\tau_p = (c/n)\alpha_i + (1/2L)ln(1/R_1R_2)$. For a cleaved cavity laser of length L = 400 μm with $R_1 = R_2 = 0.32$ and a photon absorption 5 cm^{-1}, we estimate the photon lifetime as $\tau_p = 3.6$ ps. For an InGaP/GaAs HBT with a base thickness of 1000 and a doping concentration of 10^{19} cm-3, we estimate the base transit time as $\tau_t = W_b^2/2D = 1.93$ ps. The base recombination lifetime at threshold can be estimated [10] from the current gain as $\tau_B = \beta\tau_t \approx 4$ ps. For an HBT transistor laser (TL) with stimulated base recombination, the base current and current gain can be further modified and expressed as

$$I_B \equiv I_{BTL} = \frac{Q_B}{\tau_{BL}} + \frac{Q_B}{\tau_{ST}}, \beta_{TL} = \tau_{TL}/\tau_t, \tag{4.5}$$

where Q_B is the charge stored in the base, τ_{BL} is the base recombination lifetime in laser operation, and τ_t is the base transit time and is the effective base recombination lifetime of the transistor laser including τ_{ST}, the stimulated recombination lifetime. Thus, we are able to estimate the base recombination lifetime at a given base current during transistor laser

operation from the differential beta measurements (a common microwave circuit measurement). We estimate the base recombination lifetime as τ_{BL}= 4.4 (30 mA), 5.0 (50), 5.6 (70), 5.2 (80), and 5.5 ps (90). For a damping ratio $\xi \leq \sqrt{2}$, $\omega_r = \omega_n\sqrt{1-2\xi^2}$ the resonance frequency and the resonance peak can be expressed as $M_r = 2\xi\sqrt{1-\xi^2}^{-1}$. For a damping ratio $\xi > \sqrt{2}, M_r = 1$, and $\omega_r = 0$, the modulation bandwidth (BW) can be estimated as $BW = \omega_n[(1-2\xi^2) + \sqrt{4\xi^4 - 4\xi^2 + 2}]^{\frac{1}{2}}$. These expressions and estimates lead to the calculated values shown in Table 4.1.

TABLE 4.1 Values for transistor laser with L=400 μm, I_{th}=23 mA, and operating at 15 °C.

	$\frac{I_B}{I_{th}}$	τ_p (photon lifetime) (ps)	τ_{BL} (base recomb. lifetime) (ps)	f_n (undamped natural frequency) (GHz)	ξ (damping ratio)	Calculated −3 dB bandwidth (GHz)	Measured −3 dB bandwidth (GHz)
Ground	1.3		4.4	22	1.07	12.8	2.9
state	2.2	3.6	5.0	41	0.85	32.9	7.0
First excited	3.0		5.6	50	0.85	40	10
state	3.9	3.6	5.5	61	0.93	44	13.5

It is clear that for a damping ratio $\xi > \sqrt{2}$, no resonance peak and resonance frequency ($M_r = 1$ and $\omega_r = 0$) are measured, which agrees well with the data of Figure 4.7. The intrinsic bandwidth of the transistor laser is estimated to be as high as 44 GHz in spite of the measured result of 13.5 GHz. The discrepancy arises from large parasitic capacitance and resistance values.

4.7 Voltage Modulation of Transistor Laser

Thus far, all reported direct-modulated diode and transistor lasers have employed current-driven operation. In the present work, we report sensitive structure, which is of potential use in signal mixing and processing, in the transistor laser light output (the LI-V characteristics) as a function of both base current and the collector-to-emitter voltage. The structure in the

LI-V characteristics is related to the shift in recombination from the ground to excited state of the base QW, mode changes, or shift from stimulated to spontaneous operation. The fine structure (current and voltage dependent) within the laser region of the LI-V characteristics and on the breakdown boundary offers especially sensitive bias positions for transistor laser operation, including for signal mixing and switching. As a consequence, we describe here the voltage-driven switching operation of a transistor laser employing the Franz-Keldysh photon-assisted process (under the constraint $I_E + I_B + I_C = 0$), which switches the optical and electrical operation from high coherent optical field (stimulated emission) to lower incoherent field (spontaneous emission). The TL crystal of the present work [16] is a stack of thin layers of AlGaAs, GaAs, InGaAs, and InGaP grown on a GaAs substrate by MOCVD. The critical p-type base region upward from the collector is a series of layers consisting of: (a) 21 nm of GaAs graded in doping from 8×10^{18} to 2×10^{19} cm^{-3}, (b) a 16 nm undoped InGaAs QW, and (c) 51 nm of GaAs with the acceptor doping graded from 1×10^{19} to 4×10^{19} cm^{-3} (just below the InGaP emitter).

For heat sinking reasons and convenience in cleaving, the fabricated wafer is lapped to a thickness of $\sim$ 70 μm. Experimental samples with 4 m emitter mesa widths (constricted to a 2.5 μm active width by buried edge-wise oxidation of a top AlGaAs layer) [17],[18], and with 3 μm base-contact widths at 3 μm spacing from the emitter edges, are cleaved normal to the emitter stripes to form Fabry-Perot facets with 400 m spacing. The substrate side of the TL sample is alloyed onto a Cu heat sink coated with In and mounted on a thermoelectric heater/cooler for continuous operation (cw) at 15 °C.

Figure 4.8 shows the collector I-V characteristics of a transistor laser exhibiting the considerable difference in form (e.g., gain compression) from that of an ordinary HBT operating in spontaneous base recombination. There are three distinct regions, representing different operating conditions, namely, spontaneous (region 1), QW ground-state laser operation (region 2), and first-excited-state laser operation (region 3). Near or at threshold of the first-excited-state laser, the collector current is locked (I_C = constant, $\Delta I_E = \Delta I_B$) for V_{CE}

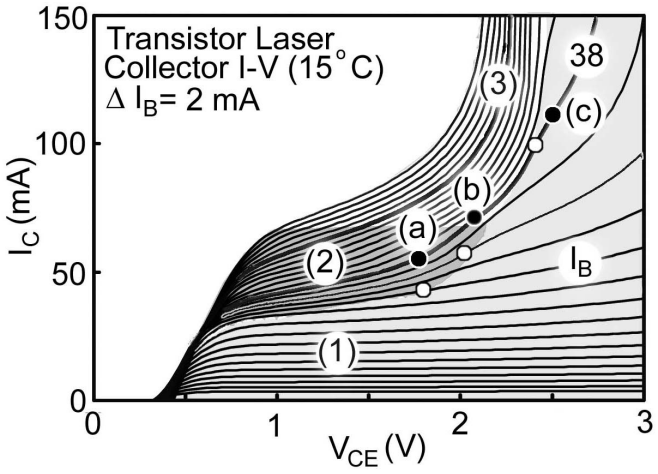

Figure 4.8: Common-emitter collector I-V characteristics of a transistor laser (I_B = 10-60 mA). Numbered regions represent different operating conditions, the spontaneous-recombination region (1), the ground-state laser region (2), and the first-excited state laser region (3). White data points outline switching from stimulated to spontaneous emission. Voltages of interest along current bias I_B = 38 mA, (a) V_{CE} = 1.8, (b) 2.2, and (c) 2.6 V.

change from 1 to 2 V and I_B >36 mA. The collector I-V characteristics are clearly distorted (bent and compressed) in the region of stimulated recombination because of the different QW ground-state and excited-state recombination lifetimes than for the usual case of spontaneous recombination [12]. The breakdown characteristics of a transistor laser of interest here are exhibited with white points in Figure 4.8 and indicate the transition (Franz-Keldysh effect, with the constraint $I_E+I_B+I_C = 0$) from stimulated to spontaneous emission [10]. Voltages of interest along I_B = 38 mA are: (a) V_{CE} = 1.8 V for the ground-state laser, (b) V_{CE} = 2.2 V for the first-excited state laser, and (c) V_{CE} = 2.6 V for spontaneous-recombination operation. The transistor laser is first a transistor and operates with three-terminals. It obeys conservation of current $I_E + I_C + I_B = 0$, with $I_C = \beta I_B$, regardless of the recombination process in the base. When V_{CE} is increased from 2.2 to 2.6 V and the base recombination switches from stimulated to spontaneous (with fixed base current I_B = 38 mA), both the emitter and the collector currents must increase. Hence, β has to increase, which is evident in Figure 4.8.

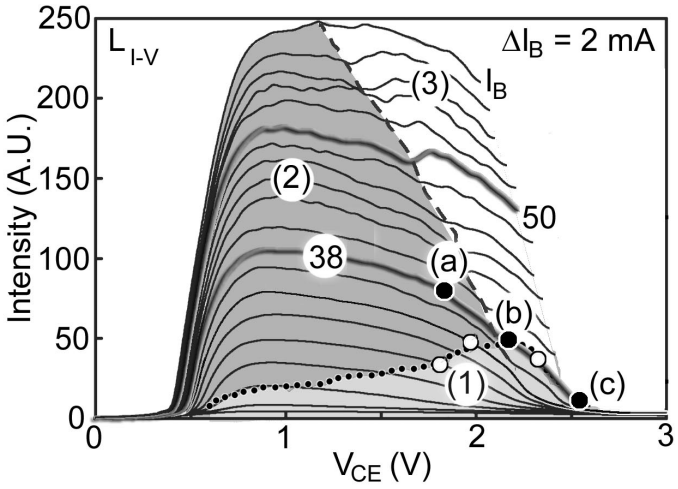

Figure 4.9: Optical output characteristics of a transistor laser at different base currents (I_B = 10-60 mA), and at collector-emitter voltages (V_{CE}) corresponding to the electrical output of Figure 4.8. White data points outline the boundary of switching from stimulated to spontaneous emission. Colored data points are voltages of interest along the constant current bias I_B = 38 mA at (a) V_{CE} = 1.8, (b) 2.2, and (c) 2.6 V. I_{TH} is determined from the correlation of optical spectra, and compression of collector I-V characteristics (gain reduction).

Figure 4.9 shows the optical output intensity of the transistor laser as a function of both base current and collector output voltage. The LI-V curve is measured using an HP 8153A lightwave multimeter. The optical intensity is directly proportional to the base recombination current, I_B, just as is the output of a diode laser to its input current. Most important, the LI-V curve reveals optical saturation and mode switching as a function of collector voltage, which, of course, is not an issue in a diode laser. The LI-V curve exhibits important features in three distinct recombination regions corresponding to the regions in the collector I-V characteristics identified in Figure 4.8, namely, the spontaneous-recombination (region 1), the ground-state laser region (region 2), and the first-excited-state laser region (region 3). At or near threshold of the first-excited-state laser (region 2 and 3), the output light intensity is linearly proportional to decreasing V_{CE} from 2 to 1 V for $I_B > 36$ mA, corresponding to the locked behavior of the collector current in Figure 4.8 (I_C = constant, $I_E = \Delta I_B$). Further increase in collector voltage beyond the gray region of Figures 4.8 and 4.9 results

in quenching of base stimulated recombination, which is caused by change of the maximum optical field to a lower average field (from stimulated to spontaneous emission). This reduces the photon-assisted Franz-Keldysh tunneling at the reverse-biased base-collector depletion region [12]. The optical field intensity shifts, coherent to incoherent (from peak field to average field), from stimulated recombination to spontaneous recombination, making it possible to increase the bias field (under the constraint $\alpha \rightarrow 1$). The shift from stimulated recombination is accompanied by a shallower increase in I_C [12]. Similar to Figure 4.8, the data points are voltages of interest along $I_B = 38$ mA, (a) $V_{CE} = 1.8$ V for the ground-state laser, (b) $V_{CE} = 2.2$ V for the first-excited-state laser, and (c) $V_{CE} = 2.6$ V for non-laser operation (spontaneous recombination). The LI-V characteristics shown in Figure 4.9 demonstrate that the optical output can be modulated by change in the collector voltage, V_{CE}, not just by current modulation.

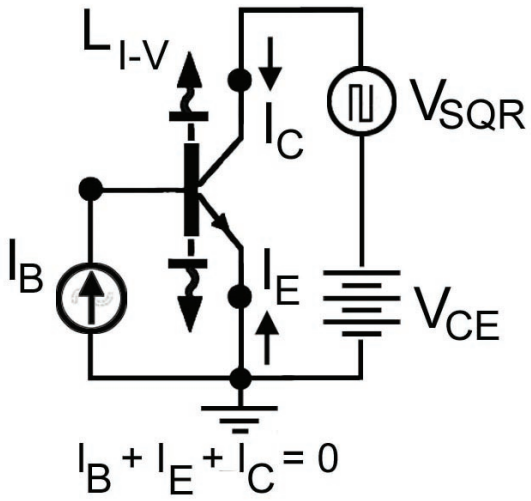

Figure 4.10: Biasing diagram for the voltage modulation (VCE) of a transistor laser.

Figure 4.10 illustrates the circuit configuration employed to modulate the transistor laser with a square wave, the voltage signal applied between the collector and emitter (CE configuration). The input is a 1 GHz square wave of magnitude 200 mV_{P-P}. DC bias is

established at a base current $I_B = 38$ mA, and collector-emitter voltages (a) $V_{CE} = 1.8$, (b) 2.2, and (c) 2.6 V. The optical spectrum of the device, operating modulated, is characterized by coupling (partially) the light into a cleaved fiber, which is fed into the monochromatic input of an HP70951B optical spectrum analyzer.

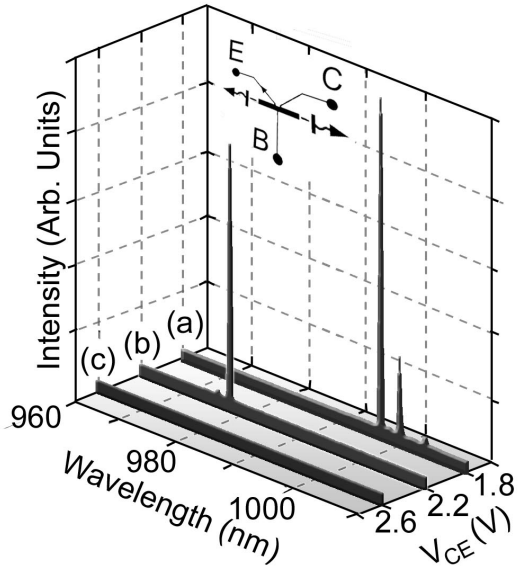

Figure 4.11: Spectral output along constant current bias $I_B = 38$ mA (Figures 4.8 and 4.9) at (a) $V_{CE} = 1.8$, (b) 2.2, and (c) 2.6 V. The input signal is modulated with a 1GHz, 200 mV_{P-P} square wave superimposed on V_{CE}.

Figure 4.11 illustrates the optical spectrum of (a) the ground-state laser at $V_{CE} = 1.8$ V, (b) the first-excited-state laser at $V_{CE} = 2.2$ V, and (c) the non-lasing state (spontaneous recombination) at $V_{CE} = 2.6$ V. The time domain optical output signal is coupled into a multi-mode fiber probe of core diameter 25 μm, and the other end of the fiber is fed into a high-speed (25 GHz) photodetector (New Focus Model 1414), with the output fed into an 18-dB-gain over 120 GHz (New Focus Model 1422) travelling wave amplifier fed into an HP oscilloscope.

Figure 4.12 illustrates the 1 GHz square wave signal at $V_{CE} = 1.8$, 2.2 and 2.6 V.

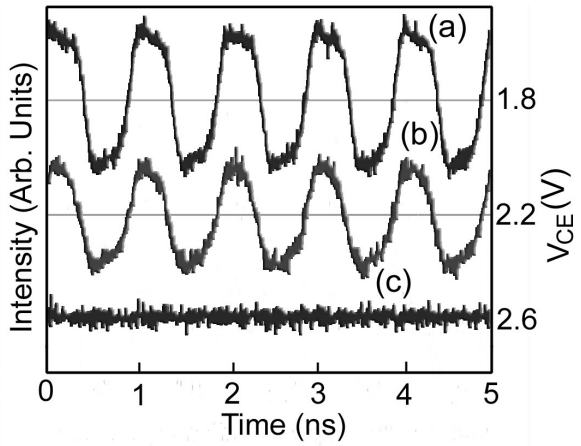

Figure 4.12: Optical output of a transistor laser with modulation at 1 GHz and V_{CE} = 200 mVP-P square wave. The C-E voltage biasing for I_B = 38 mA (Figures 4.8 and 4.9) is (a) V_{CE} = 1.8, (b) 2.2, and (c) 2.6 V.

These results clearly demonstrate the voltage-driven switching operation of a transistor laser, establishing a further class of laser signal switching.

4.8 Photon-Assisted Breakdown, Negative Resistance, and Switching in a Quantum-Well Transistor Laser

Employing both electrons and holes, intrinsically bipolar, the transistor operates by injecting minority carriers into the base (B) at the emitter (E, current I_E), recombining some of the carriers in the base (I_B = [1-α] I_E), and transporting the remainder ($I_C = \alpha I_E$, $0 < \alpha = 1$, $I_E + I_B + I_C = 0$) to the higher impedance collector (C), thus forming a transfer resistor (obviously the 1947 bipolar active device dubbed the transistor [2], the historic prototype and still relevant). In contrast to the emitter-to-collector carrier (current) transfer fraction α, the transistor common-emitter gain β can be quite large, and is $\beta = I_C$ / $I_B = \alpha$ / [1-α]. Just

from its geometry, a simple n-type slab of Ge (only a semiconductor base slab and a point contact input and output)[2], we see at once why Bardeen designated the emitter current as I_E, the base current I_B, and the collector current I_C. We see immediately, from the all-base Ge slab, that the magic of the transistor is intrinsically in the base. And, it is the base that potentially offers more, particularly when we arrive at the direct-gap, high-speed, high-current-density ($I_C \sim 106$ A/cm^2) heterojunction bipolar transistor (HBT)[6],[7], a direct descendant of the Bardeen and Brattain transistor, and realize that the base, although thin (10-100 nm), has room for more layering (bandgap and doping) and can be modified. At the high current density of the high-speed direct-gap HBT, and thus a high enough base current to be interesting (even with $\beta \sim$100), we expect significant recombination radiation. In fact, employing quantum wells (QWs) and cavity reflection, we can re-invent the base region and its mechanics (its carrier recombination and transport fraction), reduce the β gain (from $\sim$100 to $\sim$10), and achieve stimulated recombination, i.e., realize a transistor laser [9],[16]. The result is a unique transistor in form and operation, as well as a unique three-terminal laser.

Beyond a certain threshold base recombination current $I_B = I_{TH}$ (see the upper left-hand corner of the I_C -V_{CE} characteristics of Figure 4.13), stimulated recombination causes compression in the collector I_C -V_{CE} characteristics and reduction in the gain β ($\beta stim < \beta spon$). In the region of stimulated emission ($I_B > I_{TH}$, $\beta stim < \beta spon$) much more structure is evident in the I_C-V_{CE} characteristics owing to the sensitivity to QW bandfilling, state change, spectral change (coherent/incoherent, or i/c), mode-hopping (c/c), change in optical field strength, and the effect of photon-assisted collector tunneling. If the base region cavity Q (e.g., a relatively long narrow device) is spoiled, the I_C-V_{CE} characteristics revert to those of normal transistor behavior (βstim $\rightarrow$ βspon)[10] - - - revealing at once the basis of the transistor laser and how it employs carrier transport (E $\rightarrow$ C) and QW-enhanced base recombination. If the base region cavity Q (the reflection at the end mirrors) is enhanced, the transistor laser threshold ($I_B = I_{TH}$) can be reduced to quite low values before collector

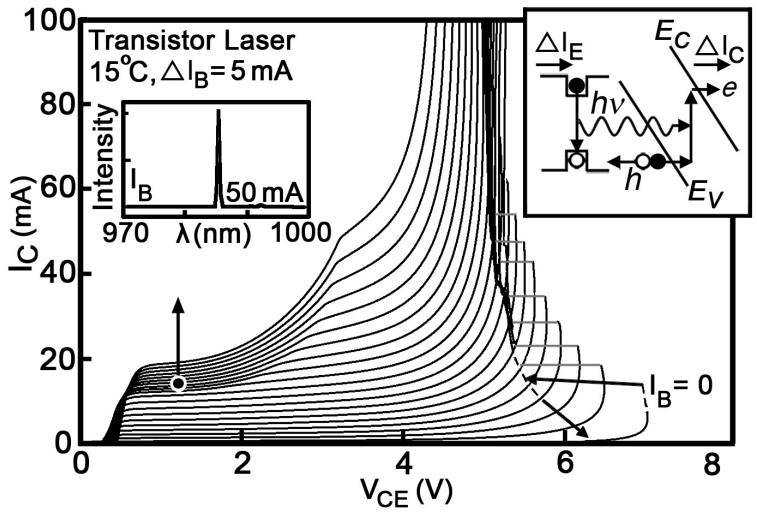

Figure 4.13: Collector $I_C - V_{CE}$ characteristics of a transistor laser with 6 μm wide emitter and 450 m Fabry-Perot cavity length operating at 15 °C. Breakdown and discontinuous switching is observed for $\alpha \to 1$ ($\alpha = \Delta I_C/\Delta I_E, I_E + I_B + I_C = 0$), from higher to lower voltage and higher current. The left-hand inset shows the laser spectrum in the lower bias (V_{CE}) gain-compression region (lower $\beta = \alpha/1 - \alpha$) at base current $I_B = 50$ mA. The diagram in the upper right inset shows the photon-assisted collector tunneling process, which releases holes for base quantum well recombination and photon generation, and thus yields the carrier-photon regeneration giving $\alpha \to 1$ and breakdown.

bias and photon-assisted tunneling cause breakdown [12]. Near the breakdown boundary, because of the bias and photon-assisted-tunneling, the device shifts from coherent to spontaneous (c/i) optical field, to lesser slope $\Delta I_C/\Delta V_{CE}$ until total breakdown at still higher voltage. At higher base currents I_B (more optical signal) it is able to switch at lower voltage from single mode (high field) to multi-mode operation (c/c) and lower average optical field. In the present paper we show that because of the three terminal device constraint, $I_E + I_B + I_C = 0$, along with the transistor switching condition $\alpha \to 1$ [19],[20], which here is a self-generated internal-feedback photon-assisted tunneling mechanism (not an avalanche or trap-filling mechanism), the transistor laser does not merely break down but switches (discontinuous) through a negative resistance region from higher voltage to lower fixed voltage and higher current, and from higher to lower optical output. At lower voltage (before breakdown) and sufficient base current I_B, instead of discontinuous switching, smooth negative

resistance ($\alpha \rightarrow 1$) is manifested in the I_C -V_{CE} characteristics at lower temperature.

The transistor lasers employed here have a current gain $\beta = \Delta I_C/\Delta I_B \sim 0.24$ below threshold, a deliberately low value in order to reduce bias-current heating. The device epitaxial layers consist of a 300 nm n-type heavily doped GaAs buffer layer grown initially, followed by a 63 nm n-type $Al_{0.40}Ga_{0.65}As$ layer, a 500 nm n-type $Al_{0.95}Ga_{0.05}As$ layer, and a 15 nm n-type $Al_{0.40}Ga_{0.65}As$ layer, all acting as lower cladding and sub-collector layers for lateral current conduction. These layers are followed by a 20 nm GaAs n-type collector contact layer, a 12 nm n-type $In_{0.49}Ga_{0.51}P$ etch-stop layer, a 60 nm lightly doped or undoped GaAs collector layer, and a 101 nm p-type AlGaAs/InGaAs/GaAs base layer, including a 19 nm lightly doped InGaAs quantum well (QW) designed for $\lambda \sim 1000$ nm. On top is a 15 nm n-type $In_{0.49}Ga_{0.51}P$ heterostructure emitter layer. The upper confining layer is completed with a 15 nm n-type $Al_{0.35}Ga_{0.65}As$ layer, a 15 nm n-type $Al_{0.80}Ga_{0.20}As$ oxidation buffer layer and a 400 nm n-type $Al_{0.95}Ga_{0.05}As$ oxidizable layer, a 30 nm n-type $Al_{0.80}Ga_{0.20}As$ oxidation buffer layer and a 50 nm n-type $Al_{0.35}Ga_{0.65}As$ layer. The top contact layer is a 100 nm heavily doped n-type GaAs. Some of the layers are used in device processing and are not important for device operation. After processing of the thin layers with various etch steps and contact metallization, the completed devices have 6 μm wide emitters cleaved to a length of 450 μm, and are capable of 10 GHz operation.

Turning first to the I_C-V_{CE} characteristics of Figure 4.13, we see in the upper left hand corner the expected compression and reduction in β gain, which agrees with the corresponding laser operation shown in the upper left inset. As shown elsewhere [10], gain compression and laser threshold can be pushed to much lower current I_B and higher voltage, perhaps eventually as far as the breakdown region (> 6 V) shown in Figure 4.13, where in the present devices further features appear, including discontinuous switching ($\alpha \rightarrow 1$, $I_E + I_B + I_C = 0$) from higher to lower voltage, and to higher current.

For example, we show in Figure 4.14 a curve-tracer plot of the $I_B = 2$ mA I_C-V_{CE} characteristic, and in the second panel the light intensity at points (a), (b), (c) and (d) of

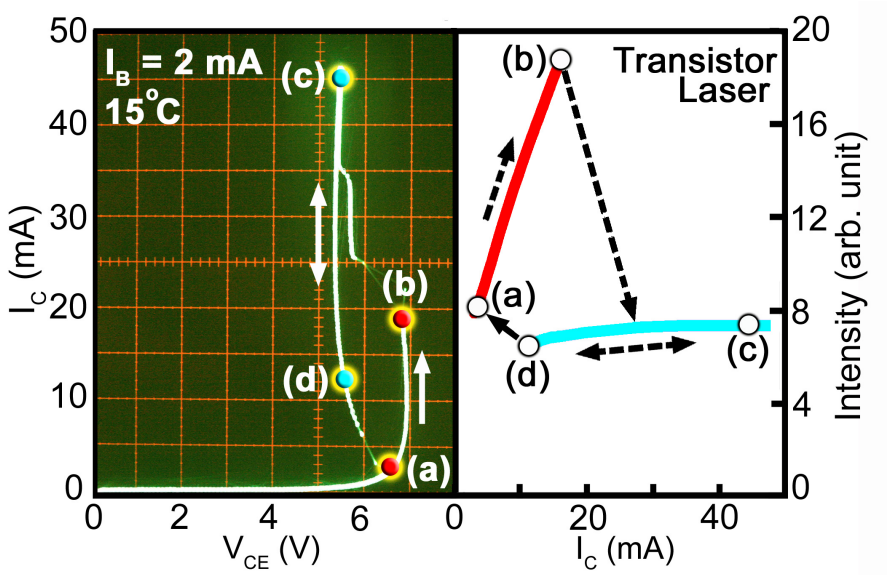

Figure 4.14: Curve-tracer plot of the $I_B = 2$ mA $I_C - V_{CE}$ characteristic of Figure 4.13 showing in detail the $\alpha \rightarrow 1$ breakdown behavior and in the second panel the light intensity corresponding to points (a), (b), (c) and (d) of the I-V trace. The light intensity from (a) to (b) agrees with $\Delta I_C = \Delta I_E = \Delta Ihv$.

the I-V trace. Before breakover, from (a) to (b), the light intensity increases progressively with I_C, but decreases after switching to lower voltage (∼7 to ∼5.5 V), and then tends to stabilize, (c) to (d), in a region of vertical I_C ($\Delta I_C = \Delta I_E$, $\Delta I_B = 0$, $\Delta V_{CE}0$), locking on $\alpha \rightarrow 1$. At higher and higher bias I_B (and more recombination radiation), the breakdown voltage V_{CE} moves inward to lower value. Note that the change in light intensity βIhv (expressed as equivalent current) from (a) to (b) agrees with $\Delta I_C = \Delta I_E = \beta I_{h\nu}$ ($\Delta I_B = 0$), which is in accord with the photon-assisted tunneling process shown in the right-hand inset of Figure 4.13.

The spectral curves (Figure 4.15) agree in amplitude with the data of the second panel of Figure 4.14 and do not vary substantially in form, as shown by the (b) and (c) normalizations in the inset. The combination of light intensity, bias voltage, and heating tend to stabilize the voltage and light intensity after switching ($\alpha = \Delta\ I_C/\Delta I_E$, $\alpha \rightarrow 1$, $I_E + I_B + I_C = 0$, $\Delta I_C\ \Delta I_E$, ΔV_{CE0}).

At lower temperature (Figure 4.16, −50 °C) the laser threshold I_B is reduced and extends

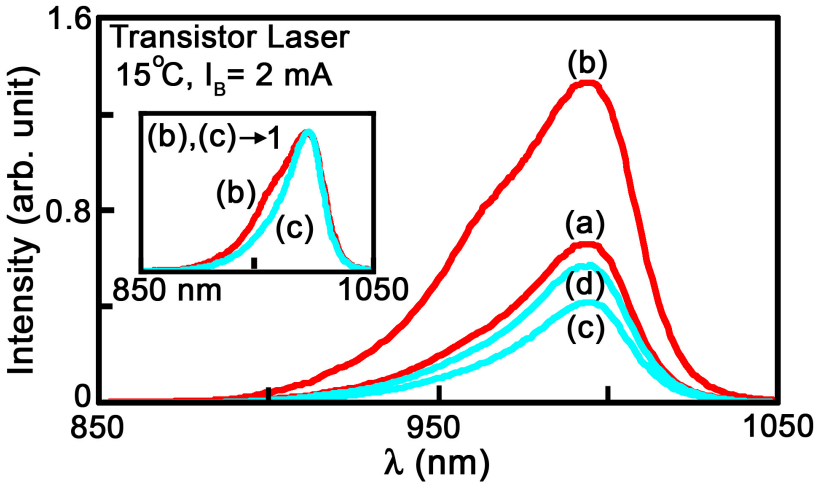

Figure 4.15: The spectral curves corresponding to the data points of the second panel of Figure 4.14. The normalized spectral curves (a) and (c) of the inset, with higher and lower intensity compared, show little change in form.

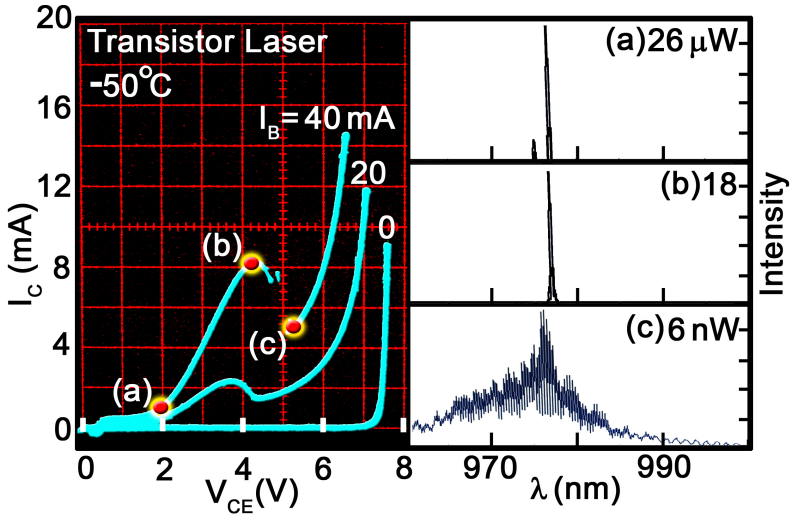

Figure 4.16: Curve-tracer plot (left panel) of the $I_C - V_{CE}$ characteristics of a transistor laser with 6 μm wide emitter and 450 μm Fabry-Perot cavity length operating at -50 °C. In the negative resistance region at $I_B = 40$ mA, between points (b) and (c), the recombination radiation changes from coherent to spontaneous and decreases in amplitude as shown by the (a), (b), (c) spectral curves on the right.

to higher voltage, to the region of the negative resistance valley of Figure 4.16. The base current I_B is an important parameter in setting the recombination-radiation level, which also depends on V_{CE}. The recombination radiation spectra at (a), (b), and (c) for $I_B = 40$ mA are shown at the right. From (b) to (c), near the valley of the negative-resistance, the recombination-radiation spectrum shifts from coherent to spontaneous (c/i) and to much lower amplitude (-30 dB), but from (a) to (b) stays coherent and reduces in amplitude only $\sim$ 1 dB. It decreases further in amplitude and broadens at higher V_{CE} (data not shown), photon-assisted tunneling playing a lesser role at lesser light intensity.

The transistor laser is unique in its capability to shift from spontaneous to stimulated base recombination ($I_B > I_{TH}$, to coherent signal), and to generate negative resistance or switch ($\alpha \rightarrow 1$, $\alpha = \Delta I_C/\Delta I_E$, $I_E + I_B + I_C = 0$) under the influence of its own optical signal. A diagram of the process in the base-collector region is shown in the right-hand inset of Figure 4.13. The transistor laser generates and regenerates its own optical signal. Photon-assisted electron tunneling (B$\rightarrow$C) at the base-collector junction re-supplies holes in the base to maintain recombination ($\Delta I_B = 0$), thus maintaining the absorption process of photon-assisted tunneling. Note that the base optical field is not decoupled; in fact, it is strongly coupled to the collector, to the tunneling, to the combined carrier-photon generation and regeneration process shown in the inset at the upper right in Figure 4.13. Recombination radiation from the base QW is the source of the photon-assisted tunneling (absorption), which feeds holes into the base to maintain recombination and leads to $\Delta I_C = \Delta I_E$ ($\alpha \rightarrow 1$, $\Delta I_B = 0$, $I_B =$ constant) and switching. If the process is tuned properly (recombination and absorption), which is self adjusting, the device sustains the process with $\Delta I_B = 0$ ($\alpha \rightarrow 1$).

In essence, the transistor laser is able to generate and regenerate photons. Depending on temperature and the device, the transistor laser exhibits (in the I_C-V_{CE} characteristics) corners, negative resistance, switching, vertical collector current (ΔV_{CE0}), spectral change (coherent/incoherent, c/i or i/c), and mode hopping (c/c) effects, all mediated by photon-

assisted collector tunneling. Among its various other properties, the transistor laser is capable of unity-alpha ($\alpha \to 1$, $\alpha = \Delta I_C/\Delta I_E$, $\Delta I_E = \Delta I_C = \Delta I_{h\nu}$) photon generation and regeneration, and consequently switching breakdown and negative resistance.

CHAPTER 5

PERFORMANCE CHALLENGES

In order to meet the challenge of a > 30 GHz directly modulated transistor laser, certain device performance criteria must be met. Previously, with a first order analysis of laser bandwidth [21]:

$$\frac{\Delta P_m(\omega)}{\Delta I_B(\omega)} = \frac{\Gamma_b \tau_p/(qAW_B)}{[1-(\omega/\omega_n)^2] + j \times 2(\omega/\omega_n)\xi}, \tag{5.1}$$

where $\Delta P_m(\omega)$ is the modulated photon density, $\Delta I_B(\omega)$ is the modulated base current, $\omega_n^2 \approx (1/\tau_p \tau_{B,spon})(I_B/I_{B,TH} - 1)$, Γ_b is the optical confinement factor of the waveguide and the damping ratio is $\xi = (2 \times \omega_n \tau_{B,spon}^{-1} + 0.5(\omega_n \tau_p)$. It is clear from this analysis that the laser bandwidth depends heavily on the threshold current, the maximum photon density, I_B, that can be driven above threshold, the photon lifetime and base lifetime. Fortunately, none of these parameters are intrinsic crystal parameters; all of them may be changed through careful process engineering.

5.1 Transistor Laser Threshold Current

One of the most important variables controlling the transistor modulation performance is the threshold current, which is dependent on many parameters:

$$I_{TH} = \frac{1}{\beta\Gamma}[\alpha_i + \frac{1}{2L}Ln\frac{1}{R_1R_2}] \tag{5.2}$$

The threshold current density depends on the internal loss α_i, the mirror reflections R_1R_2, confinement factor Γ, and the gain coefficient β. Loss α_i, depends primarily on the absorption of the photons generated in the cavity; however, it does have a component linked to the scattering and diffraction losses of the waveguide. Scattering loss is a function of waveguide roughness and is addressed in the use of a high composition AlGaAs cladding which is oxidized; the oxidation process provides an abrupt index step but also smoothes the surface due to the isotropic nature of oxidation.

The cavity length can of course be changed by cleaving the devices to different lengths and the mirror reflection can be changed by use of a deposited mirror on the device facet. Previously [12], an InGa eutectic was used as a mirror, but this is not a robust mirror which can be used to improve high speed performance; a dielectric multi-layer mirror is required.

Another crucial variable in the threshold current of the transistor laser is the device operating temperature. The thermal performance of the device, for semiconductors, is

$$I_{TH} = I_0 \exp\frac{T}{T_0} \tag{5.3}$$

The thermal stability of threshold is determined empirically and is heavily dependent on process and layout constraints.

5.2 Problem: Transistor Laser 2D Electron Gas Transport, Optical Confinement Factor and Finite Base Resistance

In a uniform base HBT, the injected electron sees a uniform mobility and is subject to diffusion and lateral electric fields (base contact to emitter edge). In order to understand carrier movement both laterally and vertically through the base, the analysis must be comprised of diffusion due to non-uniform carrier densities, lateral electric fields and carrier recombination, in short the Haynes-Shockley experiment. If we look at an emitter with width δ and begin injecting carriers into the base, the carriers will spread out from the injection point driven by a concentration gradient; they will diffuse laterally and vertically at the same rate, but will be pulled toward the base contact as the electric field created in biasing the device will act on the injected carriers. As time elapses, some of the carriers reach the collector; since the boundary condition for a collector is that there can be no excess carrier concentration, this becomes the sink for the carriers to reinforce the original diffusion. The laterally moving carriers continue to move laterally and vertically through the base until they are collected. The average time for the carrier to move from the emitter to the collector is known as the transit time. In this case the standard deviation of individual carrier lifetimes is small. In the case of uniform injection (very small intrinsic base resistance) the transit time is given as $\tau_t = X^2/(2 \times D_n)$, which uses the short base assumption to define a triangular charge population. The lateral spreading of carriers is then on the order of base length with exponential tails which spread out further. In the case of the uniform base transistor the carriers are under isotropic diffusion. A finite base resistance will change the injection concentration into the base as there will be a finite voltage drop from the edge of the emitter towards the center, forcing the injection onto the edge of the device. Finite base resistance prevents uniform carrier injection and optimum overlap with the optical waveguide. The

amount of overlap with the mesa-defined optical mode is related to the recombination lifetime of the base, the minority carrier transit time and the diffusion constant. The larger the diffusion constant and the longer the base lifetime, the more the minority carrier can diffuse to the center of the waveguide against the lateral drift. In this case this also leads to more carriers falling outside of the optically confined region (effectively using more QW volume, lower recombination density). If the recombination lifetime is reduced, the minority carrier cannot diffuse to either side of the injection edge but remains pinned to the perimeter of the device (using a lower QW volume).

The transistor laser with a quantum well in the base will behave differently. The addition of a quantum well in the base provides a high mobility channel for electron lateral transport; this differs from a HEMT device in that the device is bipolar: the channel carriers are provided by injection from the emitter rather than a built-in δ-doping. However, the mobility and transport characteristics remain similar. The lateral spreading in the transistor laser is still controlled by the lifetime in the base, but the lateral mobility in the device is much higher than the mobility seen as the electron traverses directly from emitter to collector. For instance the mobility in an $In_{0.2}Ga_{0.8}As$ quantum well can range from $\sim$ 4000 cm^2/Vs to 10000 cm^2/Vs in HEMT devices [22] near room temperature, compared to mobilities of highly-doped GaAs where $\mu_n < 1000$ cm^2/Vs [23].

Looking at the same δ width injection model for the transistor with a quantum well in the base, the injection proceeds as in the uniform base case until carriers reach the quantum well. Upon reaching the QW there is a probability for the electron to ignore the quantum well and transit as normal, or the probability for the carrier to become trapped in the well. Once an electron is trapped in the well it will move more readily with the increased mobility, laterally. The only way for the electron to move vertically through the device is to de-trap and continue through to the collector. Meanwhile the trapped carrier is sliding sideways waiting to either de-trap or recombine (Figure 5.1). Both a diffusion gradient and lateral field move carriers laterally away from the injection point. This lateral carrier movement has a large adverse

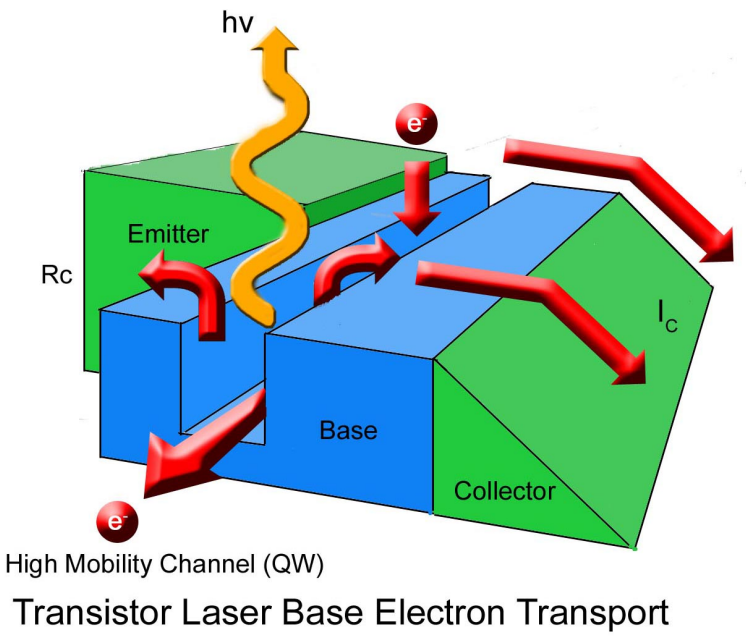

Figure 5.1: Projection schematic of electron transport in the base of a transistor laser; only the conduction band is shown.

effect on ability of the laser cavity to build up a large enough photon density to initiate the stimulated emission process (Figure 5.2), and prevents lateral scaling of the device to remove parasitics because the lateral injection can reach the base contacts (infinite recombination velocity) and cause a short-lateral base, stealing carriers from radiative recombination and increasing thermal dissipation. From device scaling experiments it is shown that there is a β gain reduction as the base contacts are moved towards the emitter due to increasing contact and surface recombination. This is also accompanied by an increase in I_{TH}.

A ridge-waveguide structure provides strong index confinement for photons; this structure is employed in the transistor laser. The ridge for the index confinement is the emitter and defines the emission geometry. As in the uniform base the resistance is not zero, forcing the injection to the edge of the emitter. With carriers being injected on the edge of the emitter traveling to the quantum well, then diffusing and drifting in the quantum well, a large

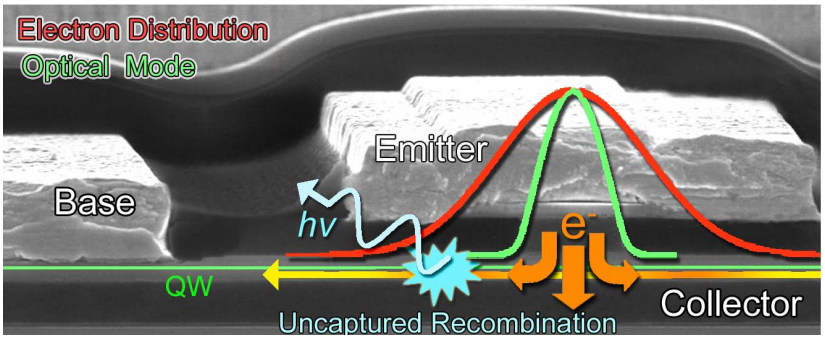

Figure 5.2: Diagram of lateral current transport in relation to the ridge optical waveguide.

fraction of carriers recombine outside of the index confinement (Figure 5.2). The fraction of the base current which recombines outside of the waveguide is lost current. If those photons were emitted into the cavity, I_{TH} would be greatly reduced.

5.3 Improvement of Optical Confinement by Extrinsic Base Zinc Diffusion

Zn diffusion into diode lasers has been used to intermix quantum wells through impurity induced layer disordering. This process takes advantage of the substitutional-interstitial nature of Zn diffusion to allow for elements in adjacent layers (different compositions) to exchange lattice sites merging the barriers into the QW. This process, if used correctly in the extrinsic base of the transistor laser, can be used to at least dope the QW, decreasing the lateral mobility of the electrons and increasing the bandgap in the extrinsic base providing a potential barrier. From the previous analysis adding a boundary condition to the lateral transport, the recombination lifetime in the non-disordered quantum well is extended by the transport in the well. Cutting off the well removes those carriers from the recombining population and instead will transport them to the collector or recombine them at the Zn disordered gap energy, effectively reducing the distribution of transit times associated with a longer diffusion constant a lateral minority carrier motion.

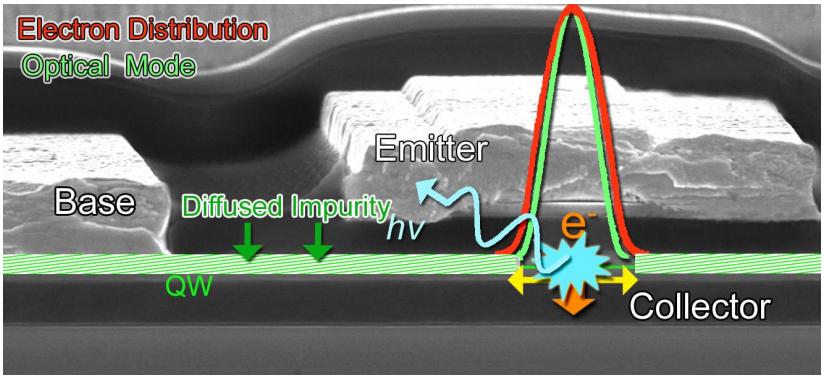

Figure 5.3: Diagram of lateral current transport in relation to the ridge optical waveguide, with extrinsic base Zn disordering.

Zn diffusion into the extrinsic quantum well will decrease both the transit and recombination lifetimes, along with increasing the overlap between the recombination region and the waveguide (Figure 5.3). Since Zn dopes heavily in GaAs $\sim 10^{20}$ cm^{-3}, diffusing Zn into the base will also lower the extrinsic base resistance, lowering the power dissipation and thus reducing the device temperature.

A Zn containing polymer film is spun onto the sample and capped with SiNx to prevent the out-diffusion of As. The sample is then heated in an open furnace tube at 650 °C for a few minutes. The resultant Zn profile was measured using ECV profiling (Figure 5.4).

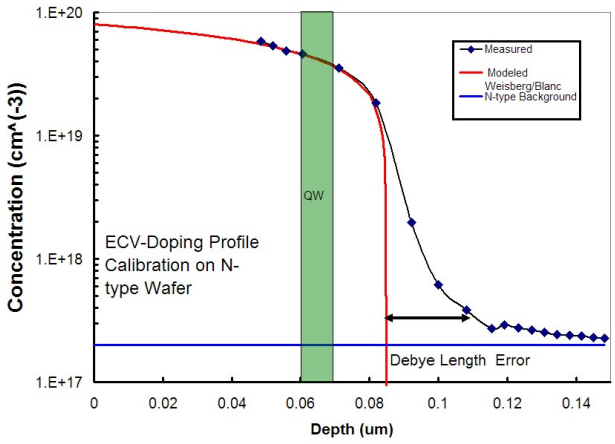

Figure 5.4: ECV calibration profile into N-type substrate.

One key constraint with the application of this process to a transistor structure is that

the diffusion cannot proceed too deep; otherwise, the base and the collector will be shorted. However, Zn diffusion results have shown an increase in transistor β, confirming that the transit time is reduced relative to the recombination lifetime (Figure 5.5) and confirming the lateral transport distance of the minority carriers. In this case the Zn was diffused 2 μm from the edge of the emitter to prevent the disordering of the emitter-base junction. On devices with faster recombination where the recombination is pinned to the injection edge, the Zn diffusion will only act to reduce extrinsic base resistance, unless the dopant can be brought close enough to the injection edge to interact with the injected minority carrier distribution.

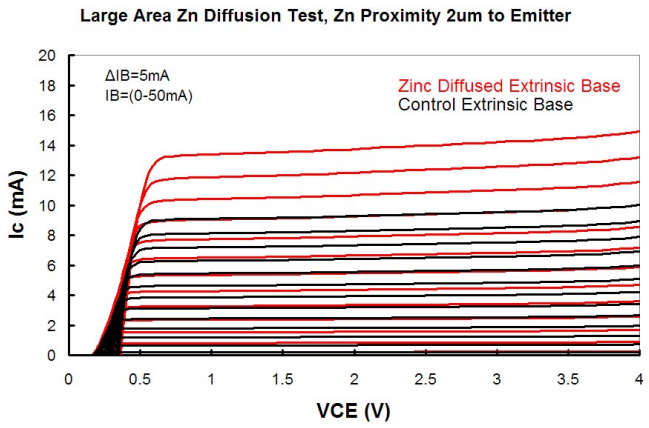

Figure 5.5: Zinc diffusion test on LET material shows an increase in device β. All other process conditions are held constant.

5.4 Problem: RF Signal Distribution

Due to the long cavity length of the transistor laser compared to the conventional HBT, speed limitations from total device parasitics are inevitable. As the signal propagates from the injection point (RF pads) two main factors determine the performance of the device, attenuation and delay. The power distribution is determined by the input impedance compared to resistance between adjacent sections of the laser. In this case the impedance looking

into the base is compared to the impedance (base resistance) looking in to the lateral distribution of the signal (finite resistance). Since the input impedance of the device is small, $\sim$ 3-5 Ω, it is not negligible compared to the metal interconnect resistance; this allows a voltage drop along the length of the device from the injection point. If the junction is not biased to the same amplitude, the emitter-base modulation current is only increased near the signal injection point. Continuing, if the modulation current is not increased, the optical power generated from the region is not increased, reducing the device optical modulation amplitude. The second problem is the phase difference between the injection point and the region of the cavity being modulated. For a quick example assume that the optical transit time is very short (modulated signal arrives at the facet instantaneously); if the device is long enough with even power distribution and the region attempted to be modulated is 180 degrees out of phase of the injection point, no output modulation is seen at the facet. This is a severe case used for illustration; however, the effect can be felt with a 20 degree phase difference. When attempting digital modulation of the laser, the result will show as an increase in jitter; this is difficult to observe as the aforementioned power distribution problem tends to be more severe along the length of the device than the phase delay (however, with the large collector-base capacitance from the 60 nm collector the phase delay is not negligible).

5.5 RF Distribution with Base Input Fingers

As a possible solution to uneven power distribution along the length of the device, multiple input fingers can be used. This approach solves both the phase delay and finite resistance problems. Since each finger originates at the same distribution node and has identical electrical length to different injection points along the device length, the phase problem is reduced to the allowable delay between regions. Using multiple injection nodes also reduces the voltage drop along the device, reducing the effect of the finite transmission line resistance. Determining the optimum number of injection nodes is dependent on the device operating

frequency as both the finite resistance and phase delay issue are frequency dependent. A second constraint is the practical distance between injection points. To keep the electrical lengths between the pads and the base injection point equal one must increase the number of series divide-by-two structures, reducing the performance advantage as the power is attenuated traversing the fan-in circuitry rather than dissipating in the device. More divide-by-two structures in series increases the device size reducing the number of devices on a die. A second process limitation is the proximity of metal regions on the same mask level. Since now the device is attached to the probe pads by an indirect smaller metallization, the thermal resistance is increased as compared to the non-distributed layout; more metal means a reduced thermal resistance. In order to reduce the impact of the distribution on the thermal performance, a "thick" metal process is required.

5.6 Problem: Transistor Laser Thermal Performance

The performance of optical devices is heavily dependent on temperature; the ohmic losses from putting current and signal into the device inevitably heat the device. To mitigate the effect of heat on the device there are two options: either prevent the heat from being generated (reduce resistances) or pull the heat away from the device. The zinc diffusion will reduce the extrinsic base resistance, reducing device heating. However, more heat needs to be pulled from the device due to ohmic losses in the emitter and collector. Previous work has been done with HBT modeling to propose the removal of heat through the emitter of the device [24]. The previous thermal analysis however does not recognize the effect of the thermal shunt contact area to the substrate; previously the thermal shunt was seen to connect through a common substrate resistance for both the heat removed from beneath the device and that removed by the thermal shunt. A GaAs substrate has relatively poor thermal conductivity and a certain thickness must be maintained for device robustness and the ability to cleave through interconnect metallization.

In order to minimize the thermal resistance of the thermal shunt, the contact area to the substrate must be large to increase the cross sectional area for read transfer. The second issue is to note the distances between the emitter and the thermal shunt substrate tie, as the thermal resistance depends on the length of the shunt and the thickness of the shunt. The thermal shunt series length can only be reduced to a certain level before the metal to metal capacitances begin to impede high speed performance. Therefore, the metal thicknesses must be increased to reduce the thermal shunt resistance without reducing microwave performance.

5.7 Thick Electroplated Au Thermal Interconnect

The evaporation of Au through a lift-off process is practically limited to a thickness of 1.5 μm as the resolution of the bi-layer resist process used decreases rapidly with bottom layer resist thickness. Not only can features not be placed in close proximity, but the monetary cost of such a process is exceedingly high. In order to solve the thermal shunt thickness problem, a thickness of > 4 μm is required. This can be solved using an electroplated metallization process. In order to electroplate Au, a seed layer must first be deposited on the substrate; second, a thick resist mold must be made using a high contrast resist capable of 4:1 aspect ratio performance when exposed on a contact aligner (one cannot move the focal plane into the resist). Once the mold is formed, the sample is immersed in a bath of Au plating solution and current is applied. The metal deposits selectively into the mold until the mold is filled when the current is removed; calibration results are shown in Figure 5.6.

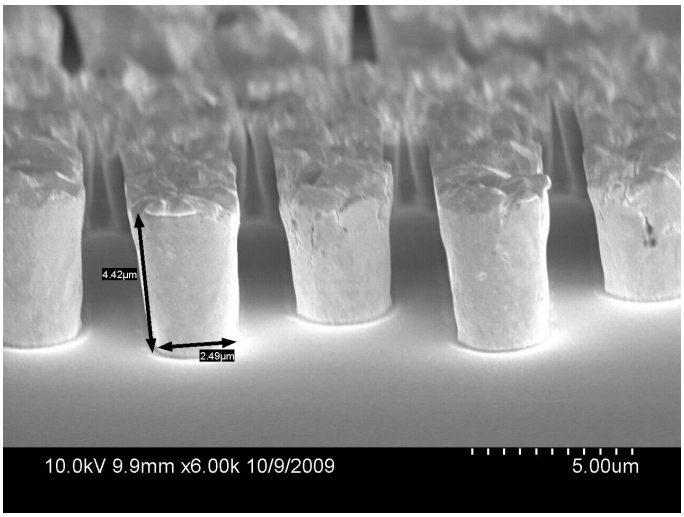

Figure 5.6: Calibration test of Au electroplating process capable of 2:1 aspect ratio metallization.

The electroplating process removes further constraints of the bi-layer metal lift-off process, allowing for the availability of completely enclosed spaces; with lift-off the "doughnut" problem can exist so that the metal cannot be lifted off as thick metal seals the resist undercut, preventing the solvent used for resist removal from entering. With this enhanced flexibility it is possible to create a completely symmetric, balanced RF-feed interconnect, as shown in Figure 5.7. The layout designed for a minimum metal overlap to maximize transmission bandwidth and maximum metal coverage of the substrate to reduce the thermal resistance is shown in Figure 5.8

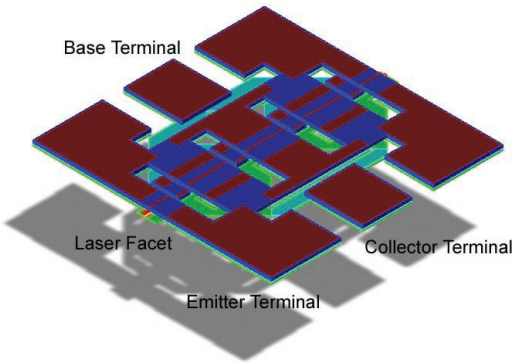

Figure 5.7: Computer rendering of layout designed to take advantage of electroplating process.

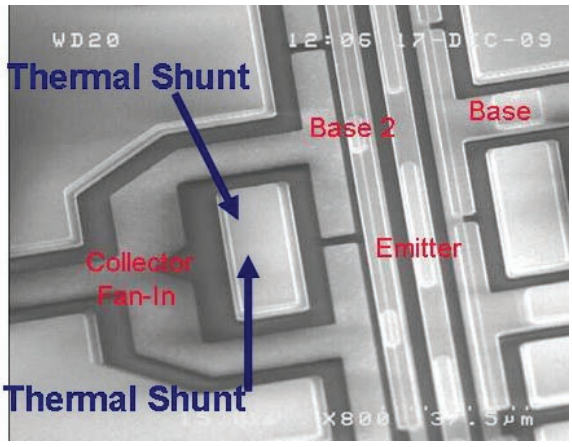

Figure 5.8: SEM micrograph of metallization with improved thermal shunting.

5.8 Problem: Reliably Controlling the Cavity Mirror Reflectance

One way to decrease threshold is to apply a dielectric mirror coating to the facet of the device. The mirror is formed by using alternating index (quarter-wavelength) materials to build up reflection at each interface. Many difficulties exist in creating a robust mirror with appropriate center wavelength. First, the laser bars must be fixtured such that the facets are exposed to the deposited film, without damaging the soft Au/polymer interconnect. The coating must have sufficient adhesion to the device facet not to peel off (Figure 5.9). In order for the wavelength of the mirror to be reproducible, the layer thickness variation must be reduced to below 10 nm, without any change in material index. Calibration mirrors on flat samples have been successfully completed and measured using a reflectometer. Currently, the main issue is the damage to device interconnect (device shorts) and mirror peeling from the surface.

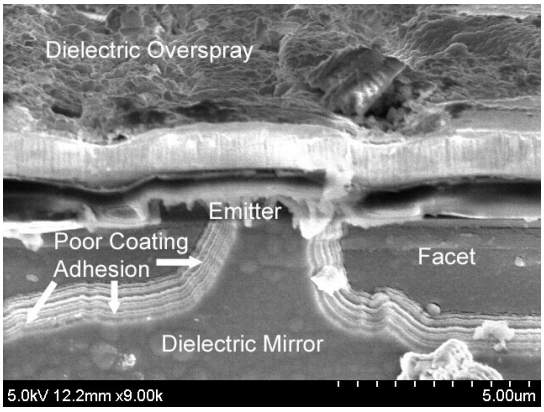

Figure 5.9: Dielectric mirror coating failure; the mirror adhesion was not sufficient.

CHAPTER 6

SECOND GENERATION TRANSISTOR LASER FABRICATION

6.1 20 GHz Process Flow

In order to improve device performance a new layout and process were designed (Figure 6.1) and implemented.

The second generation process flow begins with a SiNx hard masking of the emitter. The upper cladding is etched using a sulfuric non-selective etch; once etched, the Al bearing layers are thermally oxidized, sealing the surface against later process damage. The oxide also acts as a sidewall spacer against the following Zn diffusion step; Zn is diffused into the extrinsic base region of the device using a spin-on glass carrier, reducing the extrinsic base resistance and disordering the extrinsic base quantum well. The base is patterned and etched with citric acid, creating the mesa for Ti/Pt/Au metal deposition. Alloyed AuGe/Ni/Au collector contacts are followed by a sulfuric isolation etch down to the GaAs buffer to insure pad/device decoupling. Benzocyclobutene (BCB) is then spun onto the sample to planarize

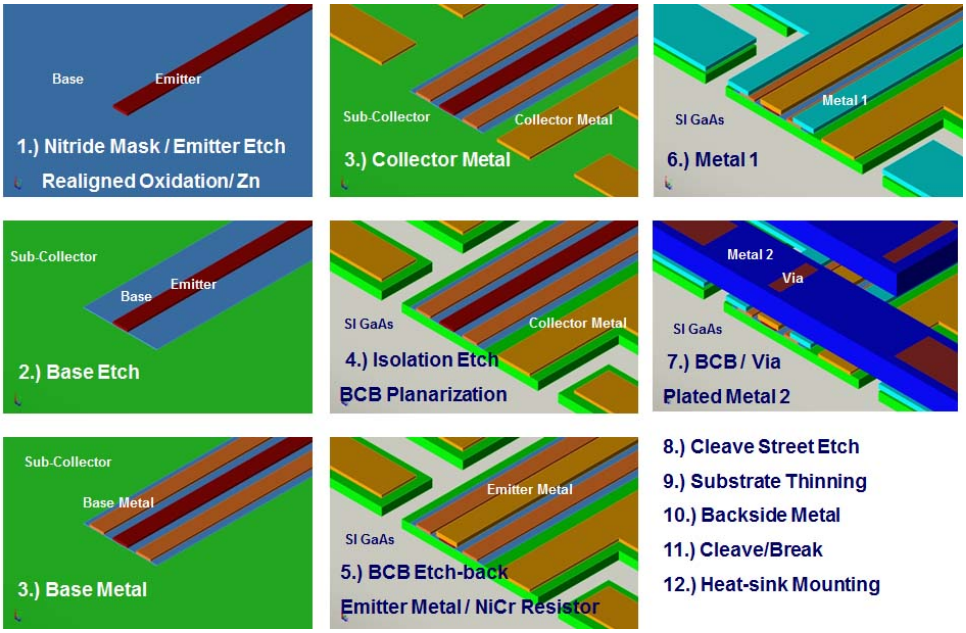

Figure 6.1: Second generation transistor laser process flow

the surface for further metallization; the BCB is etched in a CF_4 plasma exposing the GaAs capped emitter. Again AuGe/Ni/Au metal is deposited as an emitter contact, along with a first metal layer to connect the base pads to the base of the device. A second 2 μm thick layer of BCB is spun on to the sample to reduce the metal 1, metal 2 capacitance. A soft-mask is used to pattern the vias through the BCB. After the vias are etched a Ti/Au seed layer is e-beam evaporated. A 4 μm metal 2 layer is electroplated to reduce the thermal resistance from the device to the thermal shunts.

6.2 High Speed Transistor Laser Layout

In addition to the recently developed fabrication process (which minimizes the vertical overlapping capacitance), a layout which minimizes lateral capacitances, phase delays, longitudinal signal attenuation and thermal resistance is necessary (Figure 6.2) to achieve higher modulation speeds.

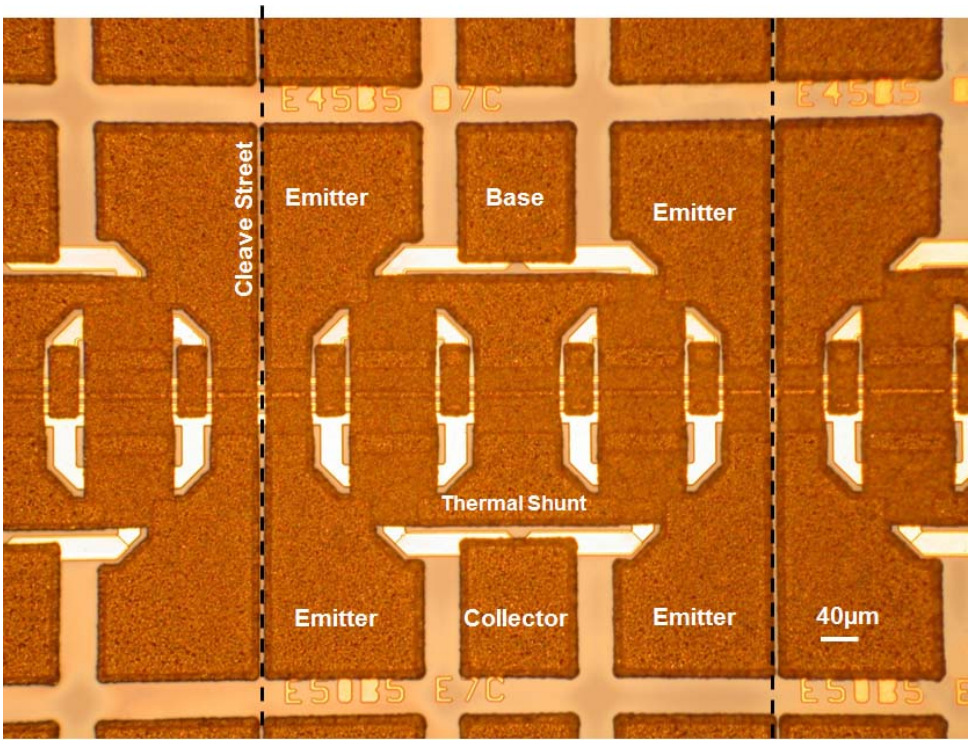

Figure 6.2: High frequency transistor laser layout with input power distribution.

CHAPTER 7

SECOND GENERATION TRANSISTOR LASER PERFORMANCE

7.1 Threshold Temperature Dependence

From the time of the invention of the semiconductor laser, operating at first cold and pulsed, 1962 [25] until the present day, temperature of optical devices has been known to determine efficiency, power consumption and general laser operating conditions. The transistor laser (TL) demonstrated at low temperature [9] (2003) achieved continuous wave operation [16] at 25 °C within a year (2004). With the improvements in process capability and layout, the operational temperature range of a single quantum-well transistor laser is increased to 55 °C. The transistor laser, unlike conventional diode lasers (using double heterojunction carrier confinement), uses essentially a single heterojunction and allows current to flow from the emitter to collector. The injected electrons not involved in the quantum-well recombination process are swept out of the base region as collector current (competing with recombination), establishing in the base a tilted (pinned not floating) carrier recombination population. The

base quantum-well provides a sufficiently fast recombination rate (spontaneous recombination lifetime < 23 ps [14]) to support laser operation above room temperature.

The TL epitaxial structure of interest here (used previously [12]) consists of a 300 nm n-type heavily doped GaAs buffer layer grown initially, followed by a 65 nm n-type $Al_{0.4}Ga_{0.6}As$ layer, a 500 nm n-type $Al_{0.95}Ga_{0.05}As$ layer, and a 15 nm n-type $Al_{0.40}Ga0.6As$ layer, acting simultaneously as lower cladding and sub-collector layers for lateral current conduction. These layers are followed by a 20 nm GaAs n-type collector contact layer, a 12 nm n-type $In_{0.49}Ga_{0.51}P$ etch-stop layer, a 60 nm lightly doped or undoped GaAs collector layer, and a 100 nm p-type AlGaAs/InGaAs/GaAs TL base layer, including a 19 nm undoped or lightly doped InGaAs quantum well (QW) designed for recombination radiation at $\lambda \sim 1000$ nm. A 15 nm n-type $In_{0.49}Ga_{0.51}P$ heterostructure is used as an emitter layer. The upper confining layer is completed with a 15 nm n-type $Al_{0.35}Ga_{0.65}As$ layer, a 15 nm n-type $Al_{0.80}Ga_{0.20}As$ oxidation buffer layer and a 400 nm n-type $Al_{0.95}Ga_{0.05}As$ oxidizable layer, a 30 nm n-type $Al_{0.80}Ga_{0.20}As$ oxidation buffer layer and a 50 nm n-type $Al_{0.35}Ga_{0.65}As$ layer. The top contact layer is 100 nm heavily doped n-type GaAs. Some of the upper layers are used for fabrication convenience and are not critical to device operation. Device processing follows standard HBT (heterojunction bipolar transistor) fabrication methods [16]. The emitter aperture is reduced through lateral oxidation [17] to a dimension of 1 μm and then cleaved to a length of 400 μm.

The I-V characteristics of a 1-μm-wide, 400-μm-long TL are shown in Figure 7.1(a) at temperature T = 10 and 40 °C. We note that a 1 μm device width for a transistor or laser is considered narrow and potentially advantageous for electrical and optical (waveguide) reasons. The distinctive collector current behavior of a TL is exhibited; typical gain compression (reduced $\beta = dI_C/dI_B$, the *signature* of a TL) [16], as the base recombination shifts from spontaneous to stimulated emission. At T=10 °C the device displays stimulated emission on two states [10], at $\lambda_0 \sim 990$ nm and $\lambda_1 \sim 980$ nm (denoted as a dashed line). As the temperature increases to T = 40 °C the collector current of the transistor increases at

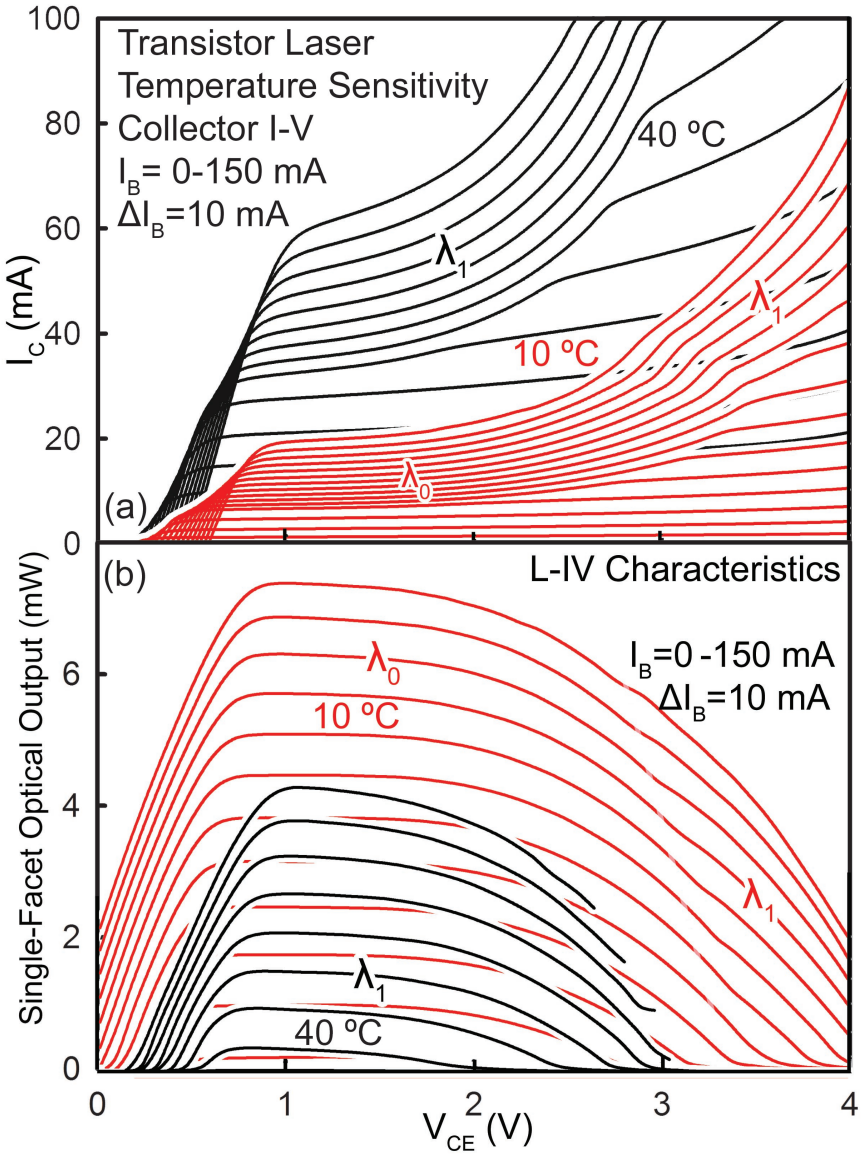

Figure 7.1: (a) Collector I-V characteristics of a heterojunction bipolar transistor (HBT) laser (1 μm width, L=400 μm) displaying increased gain with increasing temperature (10-40 °C), increased laser threshold (I_{TH} = 38 to 70 mA) and reduced laser operating range (V_{CE} > 4 to 3 V). (b) Characteristics for the same device as (a), but showing single-facet optical power shifting with increased temperature from ~7.5 to 4 mW.

the same base current I_B with optical emission exclusively from the upper state. Simultaneous measurement of the optical output (Figure 7.1(b)) of the device of Figure 7.1(a) (single facet, integrating sphere measurement) shows the complementary nature (connected) of the

optical and electrical outputs.

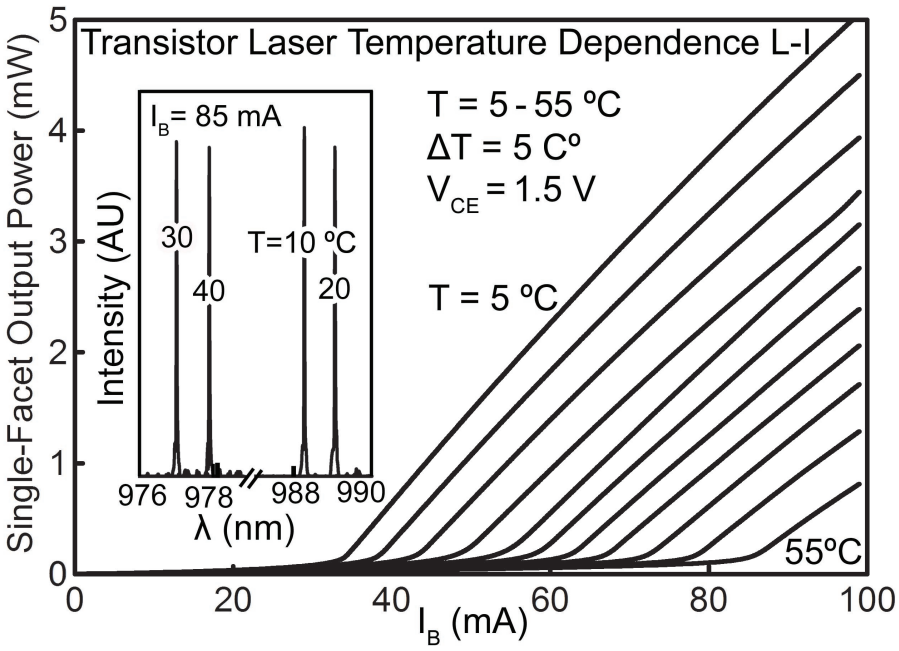

Figure 7.2: Transistor laser (TL, Figure 7.1) L-I characteristics at V_{CE} = 1.5 V as the substrate temperature is increased from 5 °C to 55 °C by increments of 5 °C. Temperature dependent optical spectra at I_B = 85 mA (inset), showing single mode operation on the lower state (10-20 °C) and the upper state (30-40 °C).

As expected, the optical power output decreases with increasing temperature, along with a reduction in the voltage range V_{CE} (V) over which the laser operates (V_{CE} reduced from >4 V to $\sim$ 3 V). To simplify the characterization of temperature effects, a low operating bias voltage of V_{CE} = 1.5 V is chosen to reduce the effect of the internal Franz-Keldysh absorption [13]. Device measurements are taken using a Peltier-stabilized thermal stage, and for effective heat-sinking the devices are thinned to $\sim$ 100 μm and mounted on an In-clad Cu heat-sink. The thermal stage is allowed a five-minute settling time to ensure stage, probe, and device equilibrium before measurements. The temperature is held within $+/-$ 0.5 °C during device operation. The TL L-I_B curves are shown in Figure 7.2 from T = 5 to 55 °C. The inset of Figure 7.2 displays the spectral output of the laser at various temperatures at I_B = 85 mA. At 10 °C the TL operates single-mode on the ground state. As

the TL is heated the spectra shift towards lower energy (longer λ) until the device switches operation to higher gain, to the first excited state, λ_1. After switching, the device returns to single-mode operation and again shifts to lower energy, until above 45 °C the spectra become multi-mode.

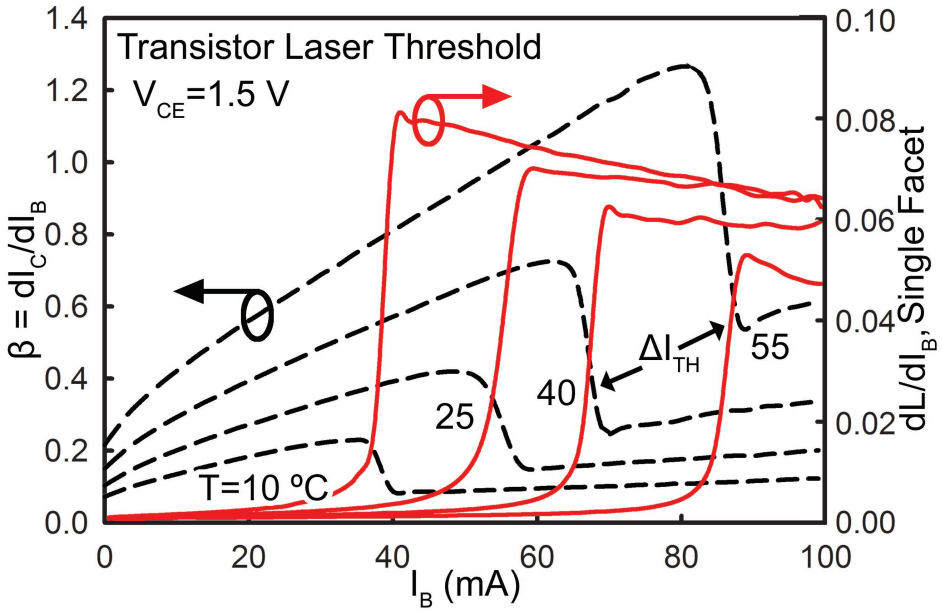

Figure 7.3: Temperature-dependent derivatives of the transistor laser (Figures 7.1 and 7.2) optical output (dL/dI_B), and electrical output (gain, $\beta = dI_C/dI_B$) at $V_{CE} = 1.5$ V. The derivatives are correlated at all temperatures; the electrical and optical performance are directly coupled.

From the L-I curves and simultaneous collector current measurements (not shown), the derivatives of the characteristics with respect to I_B can be determined (Figure 7.3). As I_B is increased, the gain ($\beta = \Delta I_B/\Delta I_C$) of the device increases up to the point of the threshold current, where the TL gain compression occurs owing to stimulated emission. The threshold current is clear from the collector output behavior without resorting to optical measurements. It can easily be confirmed with spectral measurements. L-I derivatives ensure that the electrical output is in fact in accord with I_{TH} (and laser spectra, not shown). As the temperature is increased the electrical gain increases from $\beta = 0.2$ to 1.3. I_{TH} is seen to

increase from I_B = 38 to 82 mA at 55 °C. The temperature dependence of the optical and electrical properties of the TL are tied together; the recombination rate and base transit time both variable with temperature.

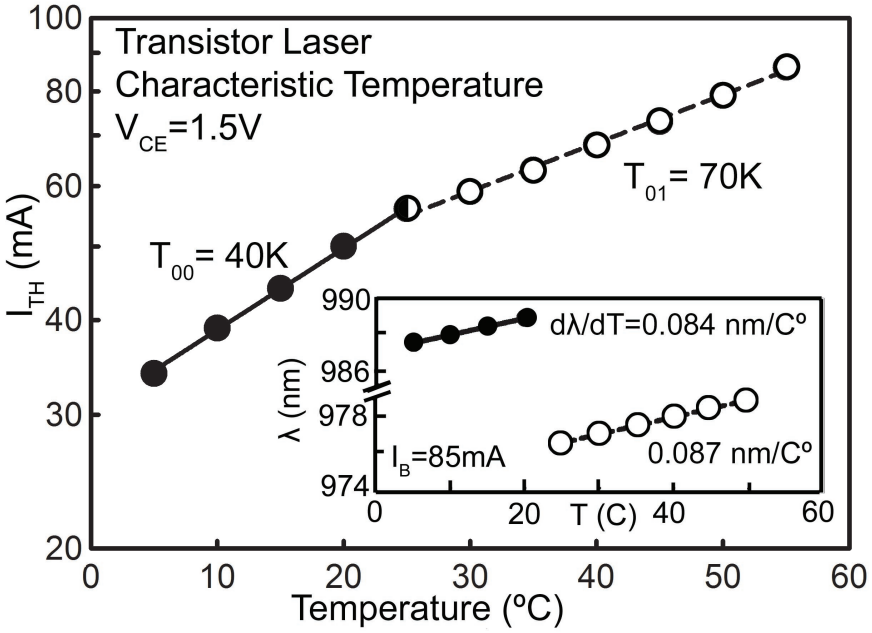

Figure 7.4: Temperature-dependent TL threshold current from 5 to 25 °C with the wavelength shifting from (λ_0) 988 nm to ∼990 nm (inset, solid). As the temperature is increased the laser changes operation from λ_0 ∼989 nm ($|0>$ state) to λ_1 ∼978 nm ($|1>$ state), shifting from λ_1 ∼ 976 nm to ∼979 nm in the range T = 30 to 50 °C, giving characteristic temperatures (from $I_{TH} = I_0(\exp T/T_0)$) to T_{00} = 40 K and T_{01} = 70 K.

The laser threshold current temperature dependence is plotted (Figure 7.4) following the usual phenomenological treatment [26], $I_{TH} = I_0 exp(T/T_0)$, and the characteristic temperature T_0 extracted. The characteristic temperatures of the ground state $|0>$ laser and that of the $|1>$ excited state are T_{00} = 40 and T_{01} = 70 K, respectively. For similar material systems with a single quantum-well device structure, characteristic temperatures for the case of diode lasers are known to vary from 50 to 120 K [27], depending on well widths and barrier heights, all within range of the present work. The difference in upper and lower state thermal stability of TL operation is connected to the difference in the corresponding density

of states and the recombination lifetimes on the lower-state ($|0>$) and upper-state ($|1>$) transitions [28]. The thermal stability can be improved from the case of the single quantum well by the addition of multiple quantum wells and graded confining layers to reduce thermionic emission from the quantum wells, in other words, with greater device (layering) refinement. Along with threshold temperature stability the spectral stability has been measured and shown in the inset. Typical wavelength shifts for Fabry-Perot resonators are 2-4 nm/°C, with external gratings often employed to reduce this spread to > 0.1 nm/°C [29]. It is evident from the low spectral shift of 0.084 nm/°C (lower state) and 0.087 nm/°C (upper state) for an as-cleaved Fabry-Perot resonator, that the TL operates single-mode on either the upper or lower state transition without the use of an optical grating. The stable single-mode operation is a property of the narrow geometry with low edge loss used for the TL current and optical confinement (i.e., the improved cavity Q). The narrow cavity is favorable not only for spectral stability but also for RF performance. The frequency response for the TL is measured at temperatures from T=5 to 40 °C. From the frequency response curves (data not shown) we are able to model the bias-dependent frequency response as a function of temperature using a photon lifetime, $\tau_p \sim 3.2$ ps, and obtain the base spontaneous lifetimes shown in Figure 7.5.

Between T = 5 and 20 °C where the TL is capable of operating on both states, the lower-state ($|0>$[14]) recombination radiation lifetime is found to vary from 122 to 132 ps. The upper-state ($|1>$) lifetime, as expected, is shorter at 83 to 88 ps. At higher temperatures >25 °C, the upper state carrier recombination lifetime varies linearly with temperature from 90 to 96 ps. Characteristic temperature differences between operation on the lower and upper state are connected to the upper- and lower- state differences in radiation recombination lifetime in addition to the relative confining barrier heights. Concluding, we show that a narrow stripe ($\sim$1 μm) transistor laser (TL) is capable of continuous wave operation up to 55 °C with output powers >7 mW per facet at a maximum frequency response of 17.4 GHz at 5 °C, reducing to 10.5 at 40 °C. The upper state and lower state of a quantum well

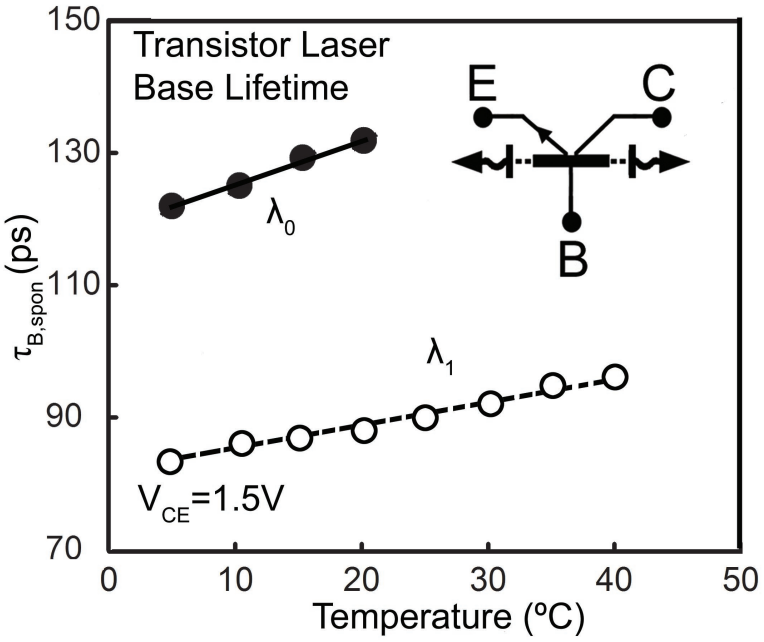

Figure 7.5: Transistor base spontaneous lifetimes for lower- and upper-state recombination radiation are extracted from bias-dependent microwave frequency response measurements of laser output across temperature from T = 5 to 40 °C. The differences in characteristic temperatures can be connected directly to the different recombination lifetimes on each state and the confining barrier heights of the lower $|0>$ and upper state $|1>$.

support different TL characteristic temperatures, with the upper-state case showing greater thermal stability than that of the lower ground state owing to different relative density of states, electron-hole recombination rates and confining barrier heights. With the narrow-stripe geometry of 1 μm, the TL operates single-mode from 5 to 40 °C at a low enough spectral shift to be useful for many purposes not requiring optical filtering.

7.2 Effect of Transistor Laser Base Recombination Lifetime on Small-Signal Bandwidth and Eye-Diagram Quality

The semiconductor laser, initially a diffused p-n junction [25], has been improved with single and double heterojunction carrier and field confinement and with active region quantum wells. Remaining in a p-n configuration until the recent addition of a quantum-well (QW) and cavity modifications to the highly doped base of a heterojunction bipolar junction transistor [10] (HBT), the HBT has now become a triode laser, a transistor laser (TL) with a tilted base carrier population favoring high speed operation. The QWHBT triode laser has demonstrated a fast spontaneous lifetime (< 30 ps) [14], a reduced photon-carrier resonance amplitude, and 20 GHz small signal modulation. The use of an asymmetrical double-heterojunction in a TL structure is investigated; introducing a small gap change at the collector to adjust and change base carrier confinement and thus change the small signal bandwidth and eye-diagram quality.

The energy band diagram for the TL structures of interest here is shown in Figure 7.6. The TL epitaxial structure consists of a 300 nm n-type heavily doped GaAs buffer layer grown initially, followed by a 500 nm n-type $Al_{0.95}Ga_{0.05}As$ layer acting simultaneously as lower cladding and sub-collector layers for lateral current conduction. These layers are followed by a 20 nm GaAs n-type collector contact layer, a 12 nm n-type $In_{0.49}Ga_{0.51}P$ etch-stop layer, a 60 nm lightly doped or undoped $Al_xGa_{(1-x)}$ As collector layer, a 100 nm p-type AlGaAs/InGaAs/GaAs TL base layer, including a 19 nm undoped or lightly doped InGaAs quantum well (QW) designed for recombination radiation at $\lambda \sim 1000$ nm. A 15 nm n-type $In_{0.49}Ga_{0.51}P$ heterostructure is used as the emitter. The upper confining layer is completed with a 400 nm n-type $Al_{0.95}Ga_{0.05}As$ oxidizable layer, used to constrict the lateral geometry. Emitter contact is made to a 100 nm heavily doped n-type GaAs layer. The emitter aperture

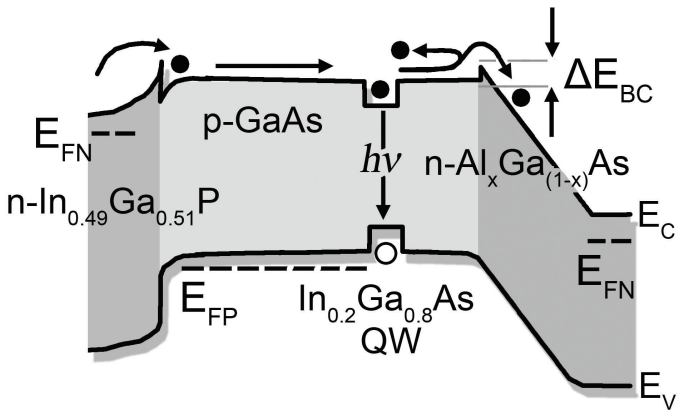

Figure 7.6: Schematic transistor laser band diagram with current blocking spike (ΔE_{BC}) at the base-collector junction.

is reduced through etching and lateral oxidation [17] to a dimension of 1 μm and then cleaved to a length of 400 μm. The two structures differ in the Al composition of the collector layer with one having an $Al_{0.05}Ga_{0.95}As$ ($\Delta E_{BC} \sim 40$ meV) composition and the other a slightly larger ($\Delta E_{BC} \sim 80$ meV) $Al_{0.1}Ga_{0.9}As$ barrier (Figure 7.6, a reflection spike).

The collector I-V characteristics (15 °C) of a 1-μm-wide, 400-μm-long TL with an $Al_{0.05}Ga_{0.95}As$ barrier are shown in Figure 7.7(a). The output signature, the β compression of transistor laser operation, is exhibited by the reduction of gain, $\beta = dI_C/dI_B = \tau_B/\tau_T$. The compression is caused by a reduction in the base lifetime, τ_B, relative to the base minority carrier transit time, τ_T, as the device shifts operation from spontaneous recombination to stimulated emission ($\tau_{sp} < \tau_{stim}$), with $I_B = I_{TH}$ =25 mA. For this device the β ranges from $\sim$ 1-3 in the region of laser operation, limiting drive currents I_B <100 mA (heating), and with, in addition, non-linearities in the I-V characteristic as I_C approaches 80 mA (solid dots). The non-linearity is due to a shift in recombination lifetime as the laser shifts oper-

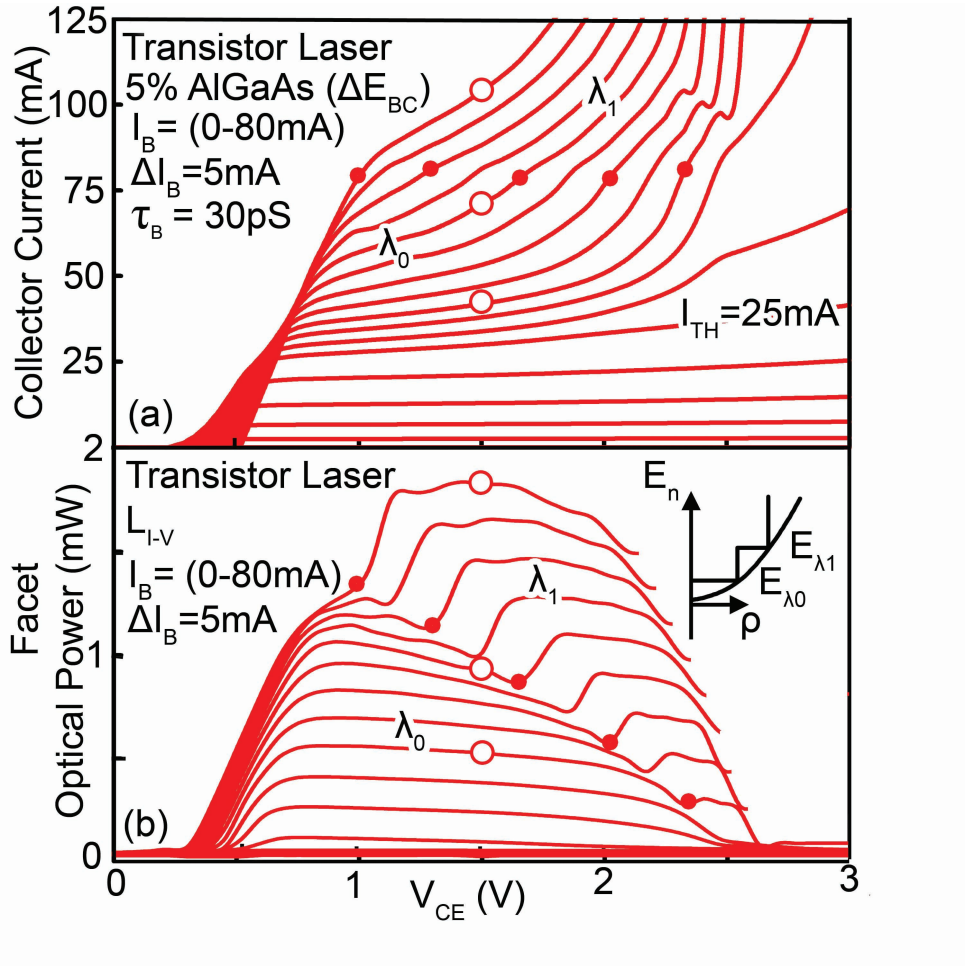

Figure 7.7: (a) Collector I-V characteristics of a heterojunction bipolar transistor (HBT) laser (1 μm width, L = 400 μm) with a GaAs/$Al_{0.05}Ga_{0.95}As$ base/collector junction. (b) Single-facet optical power for the same transistor laser device; two regions are mapped to quantum well states (inset), λ_0 ~1000 nm to λ_1 ~ 980 nm (data not shown).

ation on the QW states, with the lifetime of the upper state being shorter than the lower state (inset). The single-facet output power (integrating sphere, Figure 7.7(b)) indicates a change in device spectral operation from output at λ_0 ~1000 nm to λ_1 ~980 nm and single-facet powers in excess of 2 mW. The change in wavelength and gains are in accord with the step-like density of states of a quantum well. The optical and electrical outputs of the device are linked and complementary (solid dots).

Figure 7.8(a) shows the collector I-V characteristics of a device with the same geometry and QW design as that of Figure 7.6 except with a ΔE_{BC} ~80 meV, $Al_{0.1}Ga_{0.9}As$ barrier.

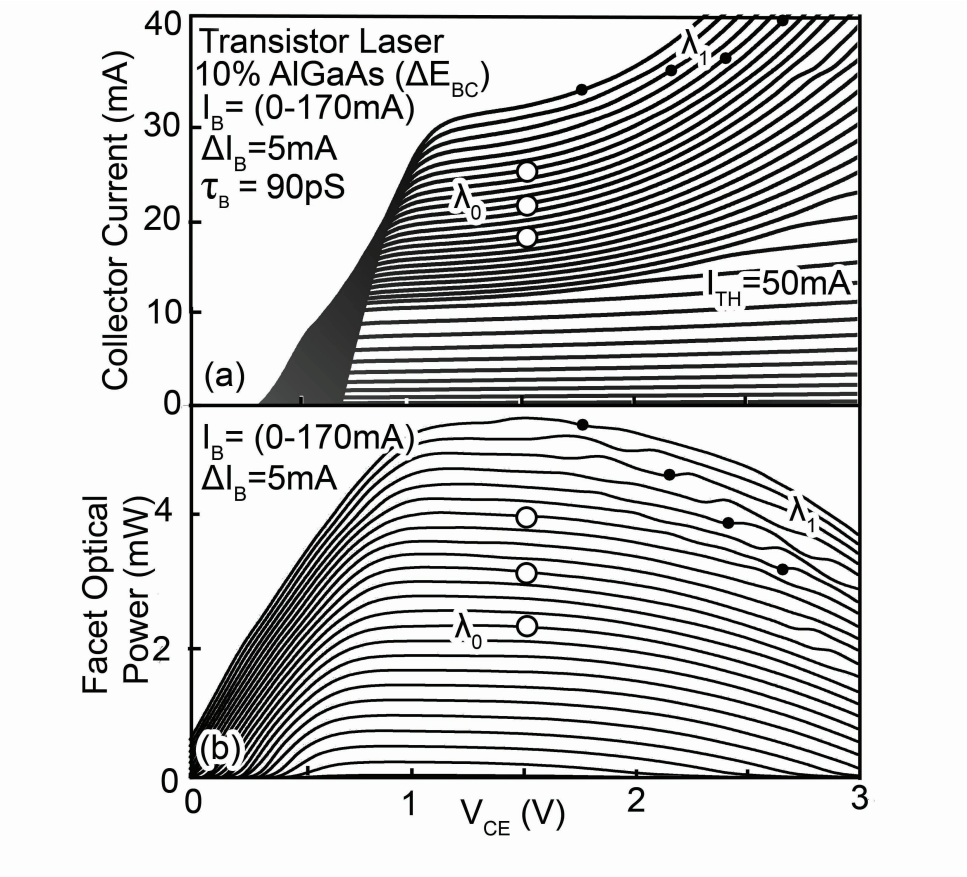

Figure 7.8: (a) Collector I-V characteristics of a heterojunction bipolar transistor (HBT) laser with a GaAs/$Al_{0.1}Ga_{0.95}As$ base/collector junction. (b) Single-facet optical power for the same transistor laser device; two regions are mapped to quantum well states, λ_0 ∼1000 nm to $\lambda_1 \sim 980$ nm (data not shown).

The effect of the blocking layer is large as β gain drops from 1-3 (Figure 7.7(a)) to $\beta < 1$, a consequence of collector current and increase in I_B. Increasing ΔE_{BC} causes the threshold current to increase to $I_B \sim 50$ mA, the maximum drive current increases to $I_B >$170 mA, and the breakdown voltage is extended to $V_{CE} > 3$ V. The TL with $\Delta E_{BC} \sim 80$ meV also shows a spectral shift, Figure 7.8(b), with operation at $\lambda_0 \sim 1000$ nm and $\lambda_1 \sim 980$ nm. The change in operation is not as easily seen from the TL I-V curve as the base lifetime is primarily controlled by the emission probability over the barrier ΔE_{BC} in addition to the QW mechanics; the stored base charge obscures the intrinsic lifetime difference between the $|0>$ and $|1>$ transitions.

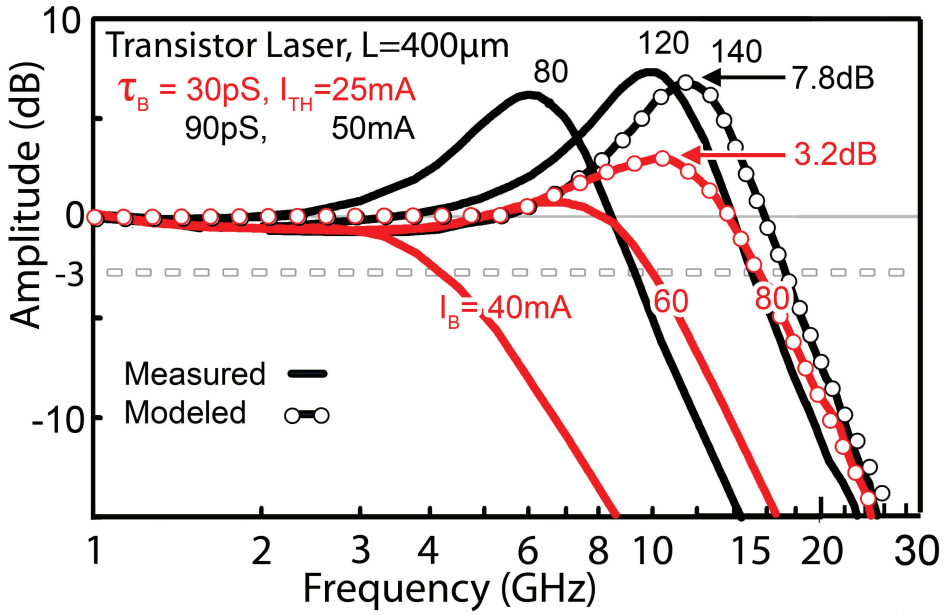

Figure 7.9: Bias dependent small signal optical bandwidth of the devices shown in Figure 7.6 (red/gray, a) and 7.7 (black, b). The red/gray curves (dotted) exhibit a 3.2 dB photon-carrier resonance which corresponds to a base lifetime, $\tau_B = 30$ ps. The black curves (dotted) demonstrate a 7.8 dB resonance and a $\tau_B = 90$ ps.

From the collector I-V characteristics, the ratio of recombination and transit lifetimes ($\beta = dI_C/dI_B = \tau_B/\tau_T$) are known, modulation data allowing determination of specific lifetimes. The small-signal bandwidth is shown for both devices (Figures 7.7 and 7.8) in Figure 7.9, with the bias points for comparison chosen to give comparable 3 dB bandwidths > 12 GHz. The bandwidth is shown at $I_B = 40$, 60 and 80 mA for the device with ΔE_{BC} 40 meV, and $I_B = 80$, 120 and 140 mA for the device with $\Delta E_{BC} \sim 40$ meV. The carrier-photon resonance amplitude for the device with an $Al_{0.05}Ga_{0.95}As$ barrier ($\Delta E_{BC} \sim 40$ meV) is 3.2 dB while the device with an increased barrier height $Al_{0.1}Ga_{0.9}As$ ($\Delta E_{BC} \sim 80$ meV) demonstrates an increased resonance amplitude of 7.8 dB. Using modified Statz-deMars coupled rate equations, we can write the optical transfer function H(ω) as

$$H(\omega) = \frac{A_0}{1 - \omega^2/\omega_n^2 + j2(\omega/\omega_n)\zeta}, \tag{7.1}$$

where $\omega_n^2 = (\eta/\tau_{ph}\tau_{B,spon})(I_B/I_{TH} - 1), \zeta = 1/(2\omega_n\tau_{B,spon}) + \tau_{ph}\omega_n/2$, and A_o is a normalization factor.

The above analysis assumes a linear increase in optical intensity which does not fit at high bias currents; in this case a second order correction is used $\omega_n^2 = (\eta/\tau_{ph}\tau_{B,spon})(I_B/I_{TH} - \kappa(I_B/I_{TH})^2 - 1)$, where κ is a fitting parameter related to a reduction of dL/dI_B with increased base current. Without the correction the rate equation over-estimates the bandwidth based on a given I_B/I_{TH}. The lifetimes modeled (Figure 7.9) are 30 ps ($Al_{0.05}Ga_{0.95}As$) and 90 ps ($Al_{0.1}Ga_{0.9}As$). The slight increase in barrier height ΔE_{BC} increases the base transit time by reflecting a fraction of the collector current, changing the probability of minority carrier collection, lengthening the radiative recombination lifetime, and increasing the carrier-photon resonance amplitude with increased barrier height (and more stored base charge). Nevertheless, even with a modest ΔE_{BC} ($Al_{0.05}Ga_{0.95}As$), the tilted-charge operation of the TL persists along with an improvement in the charge-photon TL bandwidth.

The increased resonance amplitude is an undesirable characteristic in digital optical communication links. Passive low-pass filters such as Bessel filters with a fixed cut-off frequency are commonly used to filter out the resonance frequencies and improve the eye-diagram quality. In the present case of the TL, filters are not used to demonstrate the effect of the spontaneous lifetime on the quality of the eye-diagram operating with a PRBS $2^7 - 1$ pattern at 20 Gbit/s modulation. Figure 7.10(a) shows the eye-diagram of the device with $I_B = 80$ mA, $\tau_{B,sp} = 30$ ps and the system response with the device and detector removed. The eye-diagram for the $I_B = 140$ mA $\tau_{B,sp} = 90$ ps device of Figure 7.10(b) is closed, showing overshoots of the desired bit-level, even with a larger small-signal 3 dB bandwidth. Concluding, the two transistor lasers described here with differing collector barrier heights (still a large HBT emitter-collector heterobarrier asymmetry ΔE_{BC} ~40 and ~ 80 meV) are compared, demonstrating that by adjusting the minority carrier collection in the TL, one adjusts (increases) the transit time, modifying the base recombination process and increasing the recombination lifetime from 30 to 90 ps. The change in lifetime results directly in an

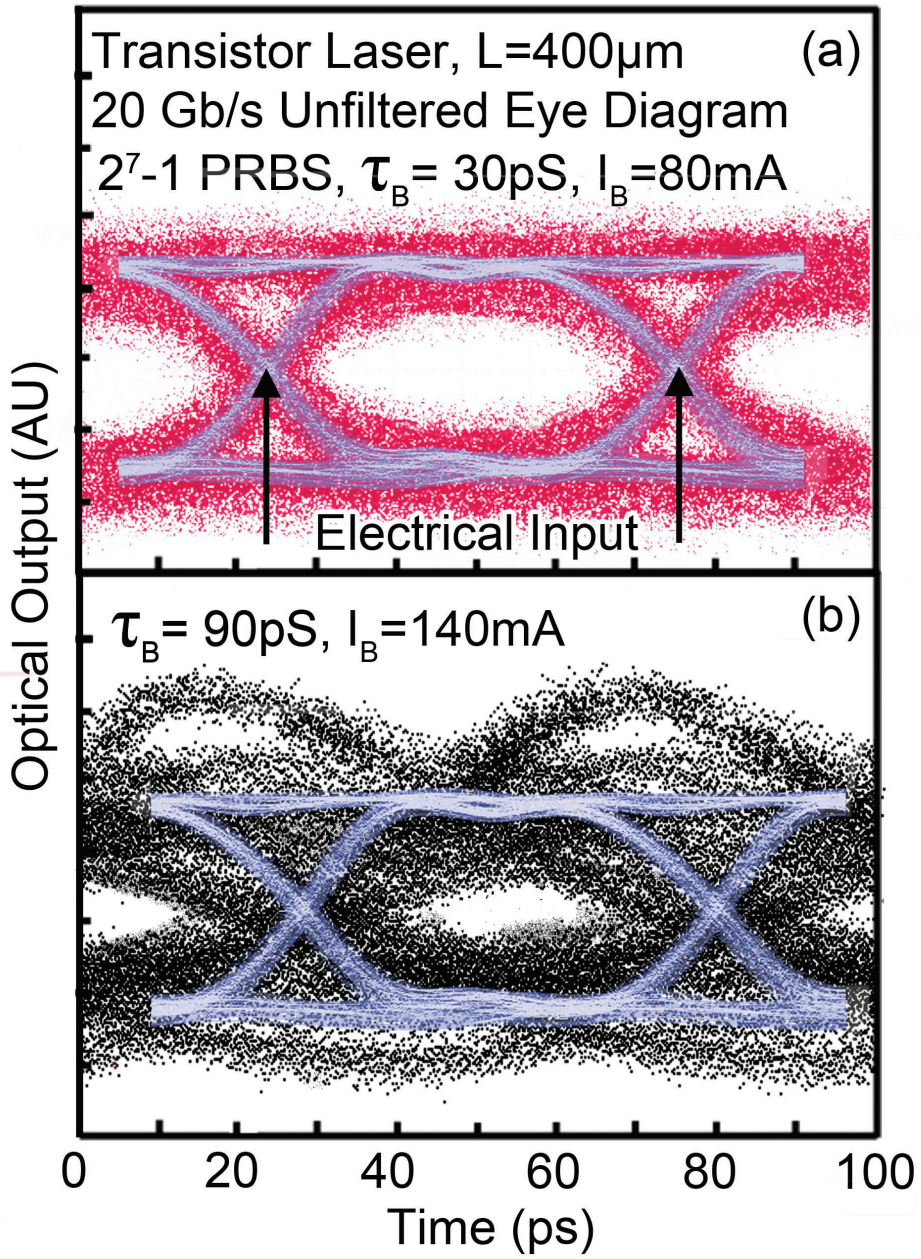

Figure 7.10: 20 Gbit/s 2^7-1 pattern length pseudo-random-bit-sequence (PRBS) measured at $I_B = 80$ mA and $V_{CE} = 1.5$ V for the device of Figure 7.6 with ΔE_{BC} ~40 meV, $\tau_B = 30$ ps overlaid with system response without TL and detector; the bit sequence is reproduced accurately and there is no overshooting of the bit amplitude. (b) ΔE_{BC} ~80 meV , $\tau_B = 90$ ps device measured at $I_B = 140$ mA; the photon-carrier resonance inserts a frequency dependent amplitude which causes overshoot and a reduction in the eye-opening.

increase in photon-carrier resonance (3.2 to 7.8 dB). Increased photon-carrier resonance is detrimental to digital modulation of the 90 ps device, greatly reducing the eye-amplitude and increasing the signal overshoot of the device. However, TL with a 30 ps lifetime shows little evidence of signal overshoot at 20 Gbit/s modulation with a PRBS $2^7 - 1$ pattern.

CHAPTER 8

SUMMARY OF WORK

Small signal bandwidth of 20 GHz and modulation of 20 Gbit/s were obtained by reducing or eliminating extrinsic parasitics which limit device performance through the optimization of device geometry and process conditions. The intrinsic recombination lifetime of the transistor laser does not limit the device performance; other problems related to parasitic capacitances, resistances, cavity losses, thermal management and maximum drive current limit the small-signal and digital large signal modulation performance. In order see the full potential of the transistor laser, these issues must be addressed; in this work a high yielding fabrication process capable of 20 GHz device performance was designed and implemented using improved lateral oxidation techniques, extrinsic base Zn doping, and 4 μm interconnect metal to reduce thermal resistance to the substrate.

REFERENCES

[1] R. Chan, "Three-port modulation of indium gallium phosphide/gallium arsenide transistor lasers," Ph.D. dissertation, University of Illinois at Urbana-Champaign, 2005.

[2] J. Bardeen and W. Brattain, "The transistor, a semiconductor triode," *Physical Review*, vol. 74, p. 230, 1948.

[3] H. Torrey and C. Whitmer, *Crystal Rectifiers*. New York, NY: McGraw-Hill, 1948.

[4] W. Shockley, *Electrons and Holes in Semiconductors*. New York, NY: D. Van Nostrand, 1950.

[5] N. Holonyak Jr. and S. F. Bevacqua, "Coherent (visible) light emission from $Ga(As_{1x}P_x)$ junctions," *Applied Physics Letters*, vol. 1, p. 82, 1962.

[6] M. Feng, N. Holonyak Jr., and W. Hafez, "Light-emitting transistor: Light emission from InGaP/GaAs heterojunction bipolar transistors," *Applied Physics Letters*, vol. 84, no. 1, pp. 151–153, 2004.

[7] M. Feng, N. Holonyak Jr., and R. Chan, "Quantum-well-base heterojunction bipolar light-emitting transistor," *Applied Physics Letters*, vol. 84, no. 11, pp. 1952–1954, 2004.

[8] N. Holonyak Jr. and M. Feng, "The transistor laser," *IEEE Spectrum*, vol. 43, p. 50, Feb. 2006.

[9] G. Walter, N. Holonyak Jr., M. Feng, and R. Chan, "Laser operation of a heterojunction bipolar light-emitting transistor," *Applied Physics Letters*, vol. 85, no. 20, pp. 4768–4770, 2004.

[10] R. Chan, M. Feng, N. Holonyak Jr., A. James, and G. Walter, "Collector current map of gain and stimulated recombination on the base quantum well transitions of a transistor laser," *Applied Physics Letters*, vol. 88, no. 14, p. 143508, 2006.

[11] J. Gibbons, *Semiconductor Electronics*. New York, NY: McGraw-Hill, 1966.

[12] G. Walter, A. James, N. Holonyak Jr., M. Feng, and R. Chan, "Collector breakdown in the heterojunction bipolar transistor laser," *Applied Physics Letters*, vol. 88, no. 23, p. 232105, 2006.

[13] C. Wolfe, N. Holonyak Jr., and G. Stillman, *Physical Properties of Semiconductors*. Englewood, NJ: Prentice-Hall, 1989.

[14] M. Feng, N. Holonyak Jr., A. James, K. Cimino, G. Walter, and R. Chan, "Carrier lifetime and modulation bandwidth of a quantum well AlGaAs/InGaP/GaAs/InGaP transistor laser," *Applied Physics Letters*, vol. 89, no. 11, p. 113504, 2006.

[15] H. Statz and G. deMars, *Quantum Electronics*. New York, NY: Columbia University Press, 1960.

[16] M. Feng, N. Holonyak Jr., G. Walter., and R. Chan, "Room temperature continuous wave operation of a heterojunction bipolar transistor laser," *Applied Physics Letters*, vol. 87, no. 13, p. 131103, 2005.

[17] J. M. Dallesasse, N. Holonyak Jr., A. R. Sugg, T. A. Richard, and N. El-Zein, "Hydrolyzation oxidation of Al[x]Ga[1-x]As-AlAs-GaAs quantum well heterostructures and superlattices," *Applied Physics Letters*, vol. 57, no. 26, pp. 2844–2846, 1990.

[18] S. A. Maranowski, A. R. Sugg, E. I. Chen, and N. Holonyak Jr., "Native oxide top- and bottom-confined narrow stripe p-n Al[y]Ga[1 - y]As-GaAs-In[x]Ga[1 - x]As quantum well heterostructure laser," *Applied Physics Letters*, vol. 63, no. 12, pp. 1660–1662, 1993.

[19] S. L. Miller and J. J. Ebers, "Alloyed junction avalanche transistors," *Bell Systems Technical Journal*, vol. 34, p. 883, 1955.

[20] J. Moll, M. Tanenbaum, J. M. Goldey, and N. Holonyak Jr., "P-N-P-N transistor switches," *Proc. IRE*, vol. 44, p. 1174, 1956.

[21] M. Feng, H. W. Then, N. Holonyak Jr., G. Walter, and A. James, "Resonance-free frequency response of a semiconductor laser," *Applied Physics Letters*, vol. 95, no. 3, p. 033509, 2009.

[22] H.-M. Shieh, C.-L. Wu, W.-C. Hsua, Y.-H. Wu, and M.-J. Kao, "Enhanced two-dimensional electron gas concentrations and mobilities in multiple d- doped GaAs/In[0.25]Ga[0.75]As/GaAs pseudomorphic heterostructures," *Japanese Journal of Applied Physics*, vol. 33, no. 4a, pp. 1778–1780, 1994.

[23] D. L. Rode, *Semiconductors and Semimetals*. New York, NY: Academic Press, 1975.

[24] W. Hafez, "Submicron scaling of indium phosphide/indium gallium arsenide heterojunction bipolar transistors toward terahertz bandwidths," Ph.D. dissertation, University of Illinois at Urbana-Champaign, 2005.

[25] R. N. Hall, G. E. Fenner, J. D. Kingsley, T. J. Soltys, and R. O. Carlson, "Coherent light emission from GaAs junctions," *Physical Review Letter*, vol. 9, p. 366, 1962.

[26] I. Hayashi, M. Panish, and F. Reinhart, "GaAs-Al[x]Ga[1-x]As double heterostructure injection lasers," *Journal of Applied Physics*, vol. 42, no. 5, p. 1929, 1971.

[27] S. D. Hersee, B. de Cremoux, and J. Duchemin, "Some characteristics of the GaAs/GaAlAs graded-index separate-confinement-heterostructure quantum-well laser structure," *Applied Physics Letters*, vol. 44, p. 476, 1984.

[28] H. W. Then, M. Feng, and N. Holonyak Jr., "Optical bandwidth enhancement by operation and modulation of the first excited state of a transistor laser," *Applied Physics Letters*, vol. 91, p. 183505, 2007.

[29] J. Major and D. Welch, "Singlemode InGaAs/GaAs distributed Bragg reflector laser diodes operating at 1083 nm," *Electronics Letters*, vol. 29, no. 24, p. 2121, 1993.